X-692-76-223

PREPRINT

NASA TM X- 71210

OBSERVATIONS AT THE PLANET MERCURY BY THE PLASMA ELECTRON EXPERIMENT—MARINER 10

K. W. OGILVIE
J. D. SCUDDER
V. M. VASYLIUNAS
R. E. HARTLE
G. L. SISCOE

SEPTEMBER 1976

GSFC — GODDARD SPACE FLIGHT CENTER —
GREENBELT, MARYLAND

OBSERVATIONS AT THE PLANET MERCURY BY THE PLASMA ELECTRON EXPERIMENT - MARINER 10

K. W. Ogilvie
J. D. Scudder
NASA/Goddard Space Flight Center
Laboratory for Extraterrestrial Physics
Greenbelt, MD 20771

V. M. Vasyliunas
Max-Planck-Institut für Aeronomie
D-3411 Katlenburg-Lindau 3
Federal Republic of Germany

R. E. Hartle
NASA/Goddard Space Flight Center
Laboratory for Planetary Atmospheres
Greenbelt, MD 20771

G. L. Siscoe
University of California
Department of Atmospheric Sciences
Los Angeles, CA 90024

ABSTRACT

Plasma electron observations made onboard Mariner 10 during its three encounters with the planet Mercury show that the planet interacts with the solar wind to form a bow shock and a permanent magnetosphere. The observations provide a determination of the dimensions and properties of the magnetosphere, independently of and in general agreement with magnetometer observations. The magnetosphere of Mercury appears to be similar in shape to that of the Earth but much smaller in relation to the size of the planet. The average distance from the center of Mercury to the subsolar point of the magnetopause is ~ 1.4 planetary radii. Electron populations similar to those found in the Earth's magnetotail, within the plasma sheet and adjacent regions, were observed at Mercury; both their spatial location and the electron energy spectra within them bear qualitative and quantitative resemblance to corresponding observations at the Earth. In general the magnetosphere of Mercury resembles to a marked degree a reduced version of that of the Earth, with no significant differences of structure revealed by the Mariner 10 observations. Quantities in the two magnetospheres are related by simple scaling laws. The size of Mercury relative to its magnetosphere precludes, however, the existence of stably trapped particle belts and of inner-magnetosphere ($L \leq 8$ at the Earth) phenomena generally. It is also expected that gradient-curvature drift and loss cone effects should be relatively more important at Mercury, but no observations bearing on these points were obtained. Due to the limited shielding provided by its relatively weak magnetic dipole moment, the surface of Mercury is

everywhere subject to bombardment by cosmic rays and solar energetic particles with energies greater than 1 MeV/nucleon. The region of potential precipitation by magnetospheric plasma particles is estimated to be a ring, roughly similar to the terrestrial auroral oval but broader and lying at lower latitudes, 50-57° on the noon meridian and 25-35° at midnight. The observed magnetospheric plasma densities are generally too high to be accounted for by any plausible ionospheric source and a solar wind origin is presumed.

I. INTRODUCTION

The Mariner-Venus-Mercury mission was carried out by using the gravitational field of Venus to direct the spacecraft so as to encounter Mercury. The goals of the mission, in order of importance, were:

1) to explore the environment of the planet Mercury.
2) to refine our knowledge of the environment of Venus.
3) to extend interplanetary observations from the orbit of Venus to a heliocentric distance of 0.46 AU.

In this paper, we describe the results of plasma measurements obtained in fulfillment of the first objective. The observations made during the interplanetary cruise, and immediately before and during the encounter with Venus, will form the subject of separate papers and will not be discussed here.

The nature of the trajectory of Mariner 10 was to approach Venus from the direction of its wake, to pass the planet, and to use its gravitational attraction to reach the orbit of Mercury. This is illustrated in Figure 1, where the trajectory is displayed as viewed from the North ecliptic pole. It was realized early in the life of the project that since the final orbital period of the spacecraft about the Sun was exactly twice the orbital period of the planet Mercury, several successive encounters were possible. Once on the correct trajectory to Mercury, encounters could, in principle, occur on every orbit of the spacecraft (every second orbit of Mercury), but the planet, which rotates three times on its axis for each two orbital periods, would always present the same aspect to the spacecraft at the time of encounter. In practice,

because of the small corrections required, close encounters could only be achieved while a supply of fuel remained, and three were made.

Figure 1 shows the path of the spacecraft, with the appropriate dates, between launch on November 2, 1973, and the second encounter with Mercury on September 21, 1974. Figure 2 shows encounter trajectories for Mercury I and Mercury III, when the spacecraft made close encounters with the planet; Mercury II, when the spacecraft made a relatively distant encounter, primarily designed to increase the television coverage of the planet in the north polar region, will be discussed later.

TABLE I

Encounter	Date	UT	Periapsis Distance
I	March 29, 1974	2046:38	1.29 Rm = 707 km altitude
II	September 21, 1974	2059:01	20.5 Rm = 50000 km
III	March 16, 1975	2239:23	1.13 Rm = 327 km altitude

Table I shows the dates, times, and periapsis distances of the three encounters. Rm = (2539 km), Mercury radius.

The plasma science instrument, which was furnished by a team of investigators from MIT, LASL, JPL, and GSFC, consisted of a rather sophisticated ion and electron analyzer observing the sunward direction, and a less elaborate electron instrument observing in the anti-sunward direction. Both of these, Figure 3, were mounted on a motor-driven scan platform, which caused their fields of view, fixed 172 degrees apart, to scan continuously about the spacecraft-sun line at rates of either 1 degree per second or 4 degrees per second, selected by ground command. The scan axis was within a few degrees of the normal to the plane of the ecliptic. All the measurements discussed in this paper were obtained at the 1 degree

per second scan rate. In the experiment design, the major purpose of the anti-sunward-facing electron analyzer was to continue determinations of the electron velocity distribution function into the anti-sunward hemisphere with sufficient accuracy to determine the heliocentric variation of the electron heat flux in the interplanetary medium. As a result of an unexplained problem, the sunward facing detector was disabled and no counts above the expected cosmic ray background were observed. The present article is based entirely upon the observations made by the anti-sunward facing electron detector. No information was obtained about the ions, either in the solar wind, the magnetospheres of the planets, or drifting from the planetary atmospheres; the electron heat flux could not be determined and the solar wind bulk speed could only be obtained to an accuracy of ± 50 km sec^{-1} (Scudder, 1976). Nonetheless, we obtained the first electron plasma observations in the vicinity of Mercury, which form the subject matter of the present article.

II. THE DETECTOR

The electron instrument, illustrated in Figure 3, was built at Goddard Space Flight Center. The instrument consisted of a hemispherical electrostatic analyzer, accepting electrons in the energy range 13 to 715 eV. This range was divided into 15 energy windows of width $\Delta E/E$ = 6.6 percent equally spaced on a logarithmic scale given in Table II.

TABLE II

Channel #	Detector A	Detector B
1	714.2 eV	687.5
2	538.4	518.3
3	404.4	489.3
4	303.8	292.5
5	228.0	219.5
6	171.6	165.2
7	129.1	124.3
8	97.2	93.6
9	73.8	71
10	55.8	53.7
11	41.8	40.3
12	30.6	29.4
13	23.9	23.0
14	18.2	17.5
15	13.9	13.4
16	0	
Solid Angle	.0662 Ster.	.0529 Ster.

The instrument was stepped continuously through the energy sequence, measuring the electron flux at each step for 0.4 seconds, so that an energy spectrum was obtained every 6 seconds. The field of view was fan-shaped, with angular extent ±3.5 degrees (FWHM) in the scan plane and ±13.5 degrees perpendicular to that plane. Every 84 seconds the deflecting potentials applied to the analyzer plates were set to zero for 6 seconds to obtain the measure of the instrumental background. At the output slit of the analyzer, which was elongated in the direction of the radius of curvature of the plates (Figure 3), 2 channel electron multipliers were

mounted. These were operated in a saturated mode, and were provided with separate charge-sensitive pre-amplifiers (sensitivity ~ 10^{-13}C) and amplifiers. Either output could be selected by ground command and passed to the body-mounted electronics box which contained control, logarithmic compression, data interfacing, and command decoding functions. To avoid switching the detector high voltage, both detectors operated all the time, so only partial redundancy was provided. In order to maintain detector saturation, and thus approximately constant sensitivity, the high voltage could be set successively at 2800, 3200, 3600, or 4000 V as the gain of the detectors deteriorated.

The analyzer and detectors were designed so that the expected detector lifetime of 10^{11} counts corresponded to 3 years operation in the solar wind. However, electrostatic charging of the spacecraft resulted in higher than anticipated counting rates at the lower energies. The instrument was on continuously during the cruise to Mercury but was off for a large part of the time between the first and second encounters with Mercury (Mercury I and II), and essentially all of the time between Mercury II and Mercury III. This program was adopted to ensure that good measurements would be obtained at the last encounter.

III. DESCRIPTION OF DATA OBTAINED AT MERCURY I AND III

The data obtained during the two near encounters with Mercury have been briefly described before (Ogilvie et al., 1974; Bridge et al., 1975; Hartle et al., 1975), but these observations are presented again here for completeness.

Measurements obtained at the first Mercury encounter are shown in Figure 4. Panel 1 shows the counting rate of 300 keV electrons reported by University of Chicago experimenters (Simpson et al., 1974). Panels 2, 3, 4, and 5 show electron plasma information, the counting rates of 688 eV, 71 eV, and 13 eV electrons and the electron number density calculated by integrating the observed electron distribution function. Panels 6 to 9 show, respectively, the magnitude, RMS variation, and azimuth and latitude angles describing the magnetic field (Ness et al., 1974, 1975a).

The spacecraft approached the planet moving along the trajectory shown in Figure 2 and until 2027 UT conditions were close to those predicted for the solar wind at 0.4 AU, with a magnetic field of magnitude about 20 gamma, a plasma bulk speed of 550 km sec^{-1} and density of 14 cm^{-3}. Between 2027 UT and 2028 UT (marked BS in Figure 4), there were three abrupt simultaneous changes in $|B|$, the plasma pressure, and also in the flux of 688 eV electrons. We interpret these changes as the signatures of passages past the spacecraft of a perpendicular shock front, similar to observations of multiple crossings of the Earth's bow shock. The character of the shock, its normal direction as deduced below from the fits to gas-dynamical theory, and the direction of the interplanetary magnetic field are consistent with this interpretation. After the

third shock transition, the spacecraft traversed a disturbed region, showing a much increased flux of electrons of energies ~ 100 eV, identified as the magnetosheath by analogy with observations at Earth (Montgomery et al., 1968; Scudder et al., 1973). The abrupt changes in the magnetic field direction and the drop in plasma pressure observed at 2037 UT are identified as passage through the magnetopause and into the magnetosphere of Mercury. From this time until the time of closest approach, the magnetic field increased in a regular way, and the plasma parameters remained approximately constant with characteristic electron energies in the range 100-200 eV. The electron energy spectra in this "cool plasma sheet" will be discussed in more detail in Section V. At 2047 UT, an abrupt drop in magnetic field and plasma pressure and the appearance of energetic particles signaled the beginning of an event which has been interpreted as analogous to a substorm at Earth (Siscoe et al., 1975). From this point to the magnetopause, the electron energy spectra peaked above the upper limit of the instrument's energy range, indicating the characteristic electron energies to be in the keV range or above. We call this electron population the "hot plasma sheet". An outbound magnetopause crossing occurred just before 2055, and a diffuse shock structure was crossed between 2057 and 2100 UT.

We find good agreement between the electron spectrometer results and those of the magnetometer in fixing the locations (discussed further in Section IV) and the character of the bow shock and magnetopause crossings. In particular, both instruments indicated a distinct thin (perpendicular) shock at entry and a pulsating (parallel) shock at exit. (When electrons are used as the diagnostic, the Earth's bow shock is a sharp and well-marked transition when the magnetic field is perpendicular to the shock normal,

but is diffuse, partly due to rapid motion, when the magnetic field is parallel to the normal (Greenstadt, 1972a and b).) The exit shock is discussed in Ogilvie et al. (1974), where it is shown that if an appropriate time scaling factor is applied, the diffuse pulsating shock observations at Mercury closely resemble observations made at Earth with a similar electron instrument. The temperature and density changes observed across the bow shock are also similar in magnitude to those observed at Earth (Scudder et al., 1973).

Four energetic particle events, labeled A, B, C, and D in Figure 4, occurred while Mariner 10 was inside the magnetosphere of Mercury, three during the disturbed interval between closest approach to the planet and the outgoing traversal of the magnetosphere. Changes in the electron spectra recorded by the present instrument during events A and B are discussed in Ogilvie et al. (1974). The subsequent interpretation of these events has proved to be difficult due to the possibility of the "pile-up" of low-energy electrons (Armstrong et al. (1975) and Christon et al. (1976)), and we shall not discuss them further here. Electron intensity enhancements upstream of the bow shock, appearing as "spikes", are evident in Figure 4 particularly at intermediate energies (71 eV). Spectra of two such upstream events are given in Figure 5, where they can be compared with observations taken in the magnetosheath. They are qualitatively and quantitatively similar to enhancements observed upstream of the Earth's bow shock; similar events were also observed at the second Mercury encounter, described in Section VII.

The electron and magnetic field data from the third Mercury encounter are shown in Figure 6. (The format is similar to that of Figure 4; however, the 13 eV channel is not shown since it appears that during the third encounter, unlike the first, only photoelectrons from the spacecraft surface are detected at these low energies. For the same reason, the electron density is more difficult to calculate and is not given in the figure.) The bow shock and magnetopause traversals are indicated, and it is immediately apparent that these coincide in the plasma and magnetic field data, as they did for the earlier encounter. The shock crossing on the entry side is diffuse, and those on the exit side are sharp, in contrast to the Mercury I encounter, presumably as a result of the change in direction of the interplanetary magnetic field. There are no impulsive changes in the magnetic field inside the magnetosphere but only a gradual increase in magnitude as the spacecraft passes near the magnetic pole at closest approach. The plasma electrons in the magnetosphere adjacent to both the entry and the exit magnetopause crossings are similar to those observed on the inbound pass of Mercury I and once again we label them the "cool plasma sheet". In the middle of the magnetosphere traversal, on both sides of closest approach, the electron intensities above 90 eV drop to very low values, sometimes to the instrument background level, the "polar low flux region". Appreciable count rates are observed below 90 eV, but are most probably photoelectrons from the spacecraft surface, observed by the instrument as the result of a 90 volt positive spacecraft potential.

Figure 7 shows the trajectories of both Mercury I and Mercury III, as viewed from the Sun, indicating where the various electron populations

were observed. The projection of the magnetic equator as determined by Ness et al. (1975) is also shown. The significance of the different populations and their relation to those of the terrestrial magnetosphere are discussed further in Section V.

Three examples of electron spectra are shown in Figure 8: (a) within the cool plasma sheet observed on Mercury III, (b) within the cool plasma sheet observed on Mercury I, and (c) within the hot plasma sheet. Also shown in (a) is a measured spacecraft photoelectron spectrum, determined in the course of spacecraft charging analysis for IMP-6 and -8 (Vasyliunas et al., 1974) and increased in proportion to the intensity of sunlight at Mercury. It is evident that the observed electron count rates below about 40 eV agree quite closely with the photoelectron spectrum; this is true throughout much of the Mercury III magnetosphere traversal. We interpret this as evidence that the spacecraft potential with respect to the plasma is some 40 eV (see, e.g., Montgomery, 1973); within the polar low flux region the spacecraft potential appears to increase up to 90-100 eV; no such correspondence is ever seen during the Mercury I encounter, indicating that the spacecraft potential throughout Mercury I remained below 13 eV. (The difference between the two may be due to a change of spacecraft surface properties with time; these are poorly known and a detailed interpretation of spacecraft charging effects is not possible at present.) Considering spectrum (a) only above 40 eV and allowing for a 40 eV shift between (a) and (b), the two spectra are quite similar in shape and absolute level, with intensities dropping off rapidly with increasing energy above a few hundred eV and densities of the order of 1 cm^{-3}. In spectrum (c), on the other hand, the intensity is still rising with increasing energy at the upper end of the instrument's range.

In short, the data from the two encounters are mutually consistent in delineating a single picture of a permanent magnetosphere of Mercury.

IV. BOUNDARY FITS

In this section, we compare the positions of the bow shock and the magnetopause of Mercury as observed by Mariner 10 with the location of the corresponding boundaries for the Earth. Our objective is to determine if the Mariner 10 boundary crossing locations, when multiplied by a suitable constant scaling factor S, can be fitted by the terrestrial boundary surface shapes.

In Figure 9 we show two determinations of the average magnetopause and bow shock boundary shapes for the case of the Earth, obtained by empirical fits to a large number of observed boundary crossings, using magnetometer data from five Explorer spacecraft (Fairfield, 1971) and plasma data from Explorer 33 and 35 (Howe and Binsack, 1972), respectively. We also present the Mariner 10 boundary crossing locations, multiplied by scaling factors of 7 (dots), 8 (crosses), and 9 (triangles). The crossing locations have been rotated into the ecliptic plane and have been corrected for aberration assuming a radial solar wind flow (in an inertial frame of reference) of 550 km sec^{-1}. (The difference in the dynamic pressure of the solar wind between two encounters implies a change in boundary distance of less than 6% and has been ignored.) The assumption of radial flow is an important one, since the undetermined solar wind direction leads to an uncertainty in our procedure. The best-determined boundary locations are the inbound bow shock and magnetopause crossings of Mercury I and the outbound bow shock crossing at Mercury III (last of three probable crossings).

It is clear from Figure 9 that the observed Hermean bow shock and magnetopause crossings agree well with a scaling of the average terrestrial boundary locations and that therefore there appears to be a close correspondence

of shape between the magnetospheres of the Earth and of Mercury. From the figure, we estimate that the scaling factor S (ratio of terrestrial to Hermean magnetospheric lengths, expressed in units of the respective planetary radii) is 8 ± 0.5; this corresponds to a distance of the subsolar point of Mercury's magnetopause $r_{SP} = 1.4 \pm 0.1\ R_M$. The quoted uncertainties result primarily from true temporal variability rather than observational errors; the terrestrial boundary crossing locations typically vary by one or two R_E from the average surfaces, as is evident from the figure of Fairfield (1971) that shows the observed crossings as well as the empirical fits reproduced here. Ness (1976) presents fits to the Mariner 10 magnetometer observations and obtains somewhat better correspondence by assuming solar wind flow from 5 degrees east of the solar direction than by assuming radial flow, the stagnation point distance of $1.45\ R_M$ and the magnetospheric scaling factor of 7.5 obtained by Ness (1976), fall within the estimated errors of the present work.

The observed magnetopause crossings can also be compared with a theoretical magnetopause surface; we have used that calculated by Choe, Beard, and Sullivan (1973). Each observed crossing then defines a value of S and a corresponding value of r_{SP}; these are listed in Table III. The agreement with both the values and the uncertainties estimated from Figure 9 is satisfactory. It should be noted that the value $S \approx 8$ obtained here is larger than that given by Hartle et al. (1975) from a preliminary analysis of Mercury III data alone.

TABLE III

Encounter	r_{SP}	S
MI	1.33	8.2
	1.33	8.2
MIII	1.39	7.9
	1.26	8.8
Average	1.33	8.3

V. COMPARISON BETWEEN THE MAGNETOSPHERES OF MERCURY AND OF THE EARTH

The magnetosphere of Mercury is evidently similar, in its gross features at least, to a scaled-down version of the Earth's magnetosphere, as has already been pointed out on the basis of both plasma (Ogilvie et al., 1974) and magnetic field (Ness et al., 1975b) observations. Both magnetospheres result from the interaction of a supersonic solar wind flow with a planetary magnetic dipole oriented at nearly 90° to the solar wind flow direction. As described in Section V, the observed locations of the Hermean magnetopause and bow shock are adequately fitted by scaling the corresponding boundary surface shapes for the case of the Earth. Here we pursue the comparison between the magnetospheres in more detail; some aspects of our discussion have been previously mentioned by Hartle et al., 1975, and Siscoe et al., 1975.

A characteristic length scale of a magnetosphere is the distance from the center of the planet to the subsolar point of the magnetopause: this length is 11 R_E ($= 7 \times 10^4$ km) for the Earth and 1.4 R_M ($= 3.4 \times 10^3$ km) for Mercury. Compared to the magnetosphere of the Earth, the magnetosphere of Mercury is thus smaller by approximately a factor of 8 in relation to the size of the planet and a factor of 20 in absolute units, and Mariner 10 observations in the Hermean magnetosphere at a distance of $x\ R_M$ should be compared with corresponding observations in the terrestrial magnetosphere at a distance of $8 \times R_E$. With this scaling, the magnetopause and bow shock locations match quite well, and, at least along the trajectory, the magnetic field patterns in both magnetospheres are nearly the same, as suggested by Ness et al. (1975) and illustrated in Figure 10. Here the observed magnetic field vectors in the X-Y plane along the trajectory of Mercury I given by

Ness et al. are superimposed on a presentation of magnetic field data for the Earth's magnetosphere given by Fairfield (1968), the scales of the two original figures having been adjusted so that the subsolar points of the two magnetopauses coincide. The magnetopause shapes of both figures were derived as statistical representations of terrestrial data and the slight discrepancy between the two is of no significance. Fairfield's data were taken at positions well below the equatorial plane; for Mercury I this is true only during the dark-side portion of the trajectory. The magnitude of the Hermean field in the "tail" region of some 40-45γ (Ness et al., 1975b) is larger than the average terrestrial value of 20-25γ roughly by the ratio of the solar wind densities at the two planets.

Considering now the electron observations, we note first that the Mariner 10 trajectories, when scaled up to the size of the Earth's magnetosphere as discussed above, correspond to traversals of the near-earth magnetotail region: the terrestrial counterpart of the trajectory of Mercury I enters the magnetosphere on the dark side at solar magnetospheric coordinates $X_{SM} \simeq -12\ R_E$ and $Z_{SM} \simeq -6\ R_E$ and travels on approximately a straight line to its dawn-side exit at $X_{SM} \simeq -6\ R_E$ and $Z_{SM} \simeq +3.\ R_E$, while at Mercury III the counterpart trajectory enters at $X_{SM} = -7.5\ R_E$ and $Z_{SM} = 3\ R_E$ and exits at $X_{SM} \simeq 0.5$ $Z_{SM} \approx +10\ R_E$. The low-energy electron morphology in the corresponding region of the Earth's magnetosphere is well known (cf., e.g., reviews by Vasyliunas, 1972, Frank, 1975):

Large electron intensities are mostly confined to the plasma sheet, which lies, on the average, between $Z_{SM} \approx \pm 3$ or $4\ R_E$, terminates on the earthward side at field lines with equatorial crossings of 7-10 R_E and extends down toward the Earth in a pair of "horns". The electron mean energy is

around 1 keV near the center of the plasma sheet and decreases to values of 100-200 eV near the edges; the electron number density near the center is typically 0.3-1 cm^{-3}; above and below the plasma sheet lie the tail lobes or the high-latitude magnetotail, characterized by very weak electron intensities. The electron populations observed by Mariner 10 during both Mercury I and Mercury III are virtually identical, in their qualitative properties at least, to those to be encountered along the terrestrial counterpart trajectories. This is illustrated in Figure 8, where we characterize the Mariner 10 observations along the two trajectories viewed from the Sun. The "cool plasma sheet" corresponds to the low-energy outer regions of the terrestrial plasma sheet, the "hot plasma sheet" to its more energetic central regions, and the "polar low flux region" to the high-latitude magnetotail.

As far as quantitative parameters are concerned, the electron mean energy in the "cool plasma sheet" at Mercury is of the order of 100-200 eV, in good agreement with the corresponding terrestrial value. The mean energy in the "hot plasma sheet" lies above the upper limit of the instrument energy range, 687 eV, and is therefore at least consistent with the corresponding terrestrial value of ~ 1 keV. The electron density values of Mariner 10, although, (as a result of spacecraft charging) not of high absolute accuracy, are consistent with terrestrial values scaled up by the ratio of the solar wind density values at the two planets (~ 5.0).

As an example, in Figure 11 we show a "cool" and a "hot" plasma sheet spectrum obtained at Mercury I, compared with sample one-hour-average "quiet" and "active" spectra obtained in the plasma sheet of the Earth near local midnight by the Los Alamos experiment on IMP-6 (E. Hones,

private communication). The general similarity of shape is clear, as well as the higher absolute intensity at Mercury; reflecting the larger solar wind density at 0.45 AU.

In summary, as far as plasma electron and magnetic field observations are concerned, the magnetosphere of Mercury appears to be, to a remarkable extent, simply a miniature of the magnetosphere of the Earth. The observed boundary crossings, magnetic field directions, and the location and properties of the various electron populations are all consistent with this analogy. The scaling laws appear to be the following: length reduced in proportion to the distance of the subsolar magnetopause (which is determined by pressure balance between the solar wind and the planetary dipole); electron energy unchanged; number density increased in proportion to the solar wind density and magnetic field magnitude increased in proportion to the square root of the solar wind density (therefore leaving the Alfvén speed unchanged). The solar wind velocity is unchanged and so is, presumably, the flow velocity in the magnetosheath. Siscoe et al. (1975) have shown that the analogy between the two magnetospheres can be carried even further to encompass time-varying phenomena. With all the velocities unchanged, one expects time intervals to scale in proportion to the (absolute) length. Thus, time intervals at Mercury should be reduced by a factor of ~ 20 compared to the Earth; the 1-hour substorm time at the Earth then becomes ~ 3 minutes at Mercury, in good agreement with the independent estimate of Siscoe et al.

Of course, there are aspects of the Hermean magnetosphere that differ from their terrestrial counterparts. The first and most obvious difference is the size of the planet relative to its magnetosphere. The volume

occupied by the planet Mercury corresponds to a sphere of radius 7 or 8 R_E in the terrestrial magnetosphere. Thus, firstly, the entire inner magnetosphere of the Earth has no Hermean counterpart. In particular, there should be no stably trapped radiation belts at Mercury since few if any closed particle drift orbits are expected to exist which do not intersect either the surface of the planet or the magnetopause and do not allow escape into the magnetotail, a conclusion already reached by energetic particle (Simpson et al., 1974) and magnetometer (Ness et al., 1975a) experimenters. The complicated spectral effects associated with differential plasma drifts around the Earth, extensively studied from synchronous satellites (DeForest and McIlwain, 1971) and Explorer 45 (Smith and Hoffman, 1973; Konradi et al., 1973), as well as the symmetric ring current and associated phenomena, should likewise be absent at Mercury.

Secondly, Mercury with its rotation period of 58 days is a non-rotating planet for all practical purposes as far as the magnetosphere is concerned. However, rotation is not a dominant factor in the Earth's magnetosphere, either; its most important consequence, the plasmasphere, is mostly confined to distances of less than 7 R_E, a volume of the magnetosphere that at Mercury would lie within the planet's interior. Hence, one does not expect significant differences between the two magnetospheres to arise from the existing differences of planetary rotation.

Thirdly, the electrical conductivity at the base of the magnetosphere may be different in the two cases, with important implications for possible magnetospheric convection processes. In the case of the Earth, the conducting ionosphere separated by the insulating atmosphere from the highly conducting

Earth does not impede magnetospheric convection but exerts a significant influence on its pattern (see, e.g., reviews by Vasyliunas, 1975a; Wolf, 1975; and references therein). The corresponding conditions at Mercury are highly uncertain. A Hermean ionosphere has not been directly detected (Howard et al., 1974; Hartle et al., 1975), and the outermost layers of the planet itself, if similar to those of the Moon, are likely to be poor electrical conductors. Both these factors argue for a low integrated conductivity at the base of magnetospheric field lines. However, the Earth's ionosphere is also a relatively poor conductor as far as its effect on large-scale convection is concerned (Vasyliunas, 1975b); the dimensionless ratio which measures the effect of the integrated ionospheric conductivity Σ, $4\pi \Sigma V_A/c^2$ in Gaussian units with V_A the Alfvén speed in the outer magnetosphere, is usually less than 1. Hence, no large differences between the two magnetospheres are expected here, either, unless the surface properties of Mercury are vastly different from what is usually assumed.

The weakness of the Hermean ionosphere also means that it is not a significant source of plasma for the magnetosphere; this is discussed in more detail in Section VII. Whether this implies any major differences between the two magnetospheres is not clear, since the relative contribution of the solar wind and of the ionosphere as sources for the plasma in the Earth's magnetosphere remains a major unresolved question.

Fourthly, the scaling relations given earlier do not preserve the ratio of gyroradius to length scale: at corresponding points in the magnetosphere, since this ratio is larger at Mercury, finite gyroradius effects are more important at Mercury than at the Earth. In particular, gradient drifts are more important, for the same particle energy, relative to $\mathbf{E} \times \mathbf{B}$ drifts,

and particles convected from the magnetotail will therefore penetrate less deeply into the dipolar magnetic field. The equatorial distance L_A to the boundary of closest penetration, i.e., the Alfvén layer, can be estimated by balancing the ExB drift produced by a cross-tail potential Φ_T against the gradient drift in a dipole field (treating, for simplicity, equatorial particles only). The result is

$$\left(\frac{L_A}{L_o}\right)^4 = \frac{1}{12}\,\frac{e\Phi_T}{K_o}$$

where L_o is the distance corresponding to the edge of the dipolar region ($L_o = 11\ R_E$ for the Earth, $L_o = 1.4\ R_M$ for Mercury), K_o is the particle kinetic energy at L_o (the energy varies with distance by virtue of the first adiabatic invariant), and the width of the magnetotail has been assumed to be $4\ L_o$. For plasma sheet electrons, $K_o \sim 1$ kV. At the Earth, $\Phi_T \approx 50$ kV, giving $L_A \approx 0.7\ L_o \approx 8\ R_E$.

To make a corresponding estimate for Mercury, one needs to estimate Φ_T. Dimensional analysis gives

$$e\Phi_T \approx V_{sw}\, B_{tsw}\, R_m\, \Psi\,(M_{sw}, \Theta)$$

where the subscript sw indicates solar wind values, $\underset{\sim}{V}$ is the flow velocity, B_t the magnetic field transverse to $\underset{\sim}{V}$, M the Alfvén Mach number based on B_t, Θ the angle between $\underset{\sim}{B}_t$ and the planet's dipole moment, R_m the radius of the magnetosphere and Ψ a dimensionless function (cf. Gonzalez and Mozer, 1974; Sonnerup, 1974a and b; Vasyliunas, 1974). In the solar wind, B_t varies with heliocentric distance r as 1/r while V and M are independent of r; thus, Φ_T varies in proportion to R_m/r. On this basis, $\Phi_T \approx 7$ kV at Mercury.

This result has several implications; for example, the distance of closest penetration of plasma sheet electrons is $L_A \approx L_o = 1.4\ R_M$, corresponding to 11 R_E at the Earth; particles convected from the magnetotail of Mercury should be unable to reach field lines with equatorial crossings smaller than approximately the distance to the dayside magnetopause. Secondly, the result indicates that the plasma sheet electron energy does not scale with the cross-tail potential: the energy is the same in the two magnetospheres, in agreement with observations, while the cross-tail potentials differ by a factor of 8. This also points up another possible difference between the two magnetospheres. The ion average energy in the terrestrial plasma sheet is typically 8-10 keV; if the ions had the same energy at Mercury, the energy would be comparable to or larger than $e\Phi_T$. Now as long as the particle kinetic energy K is less than $e\Phi_T$, their motion is influenced by the electric field and the value of the cross-tail potential itself has little effect; this is no longer true if $K \geq e\Phi_T$. We may anticipate, therefore, that the ion population in the Hermean magnetotail may exhibit significant differences from the terrestrial case; unfortunately no information bearing on this point could be obtained from Mariner 10. The non-scaling of gyroradius effects also implies that particle-wave interaction processes, which are strongly influenced by the size of the gyroradius compared to fluctuation wavelengths, may also be quite different in the two magnetospheres.

Finally, the much weaker surface magnetic field of Mercury implies that the size of the loss cone at any point in the magnetosphere is larger

than in the case of the Earth and consequently particle loss processes are potentially more important. As an example, we compare the minimum loss time (under strong pitch-angle diffusion conditions) required to empty electrons out of a plasma sheet flux tube with the convective flow time through the plasma sheet (see, e.g., Kennel, 1969, for extensive discussion and application of these concepts in the Earth's magnetosphere). The minimum loss time from a magnetotail flux tube is given by

$$\frac{1}{\tau_\ell} \approx \frac{1}{4} \frac{v}{L} \frac{B_z}{B_s}$$

where v is the mean electron speed, L the length of the field line, B_z the normal component of the magnetic field at the neutral sheet, and B_s the field strength at the surface of the planet. The flow time is given by

$$\frac{1}{\tau_f} \approx c \frac{E}{B_x Z}$$

where E is the cross-tail electric field, B_x the tail magnetic field, and Z the thickness of the plasma sheet. We then obtain the ratio

$$\frac{\tau_\ell}{\tau_f} \approx 4 \frac{L}{vZ} \frac{cE}{B_z} \frac{B_s}{B_x} = \frac{4L}{Z} \frac{V_x}{v} \frac{B_s}{B_x}$$

where V_x is the earthward flow speed at the center of the plasma sheet. In the Earth's magnetosphere, with $Z \approx 3\ R_E$, $L = 15\ R_E$, $B_s/B_x \approx 2 \times 10^3$, v corresponding to 1 keV electrons, and V_x varying between 100 and 500 km sec^{-1}; we obtain τ_ℓ/τ_f between 200 and 1000; the minimum loss time is much longer than the flow time and the loss of particles is therefore negligible. For Mercury, on the other hand, $B_s/B_x \approx 20$; assuming that Z and L scale by the common factor and that the velocities are unchanged, we obtain τ_ℓ/τ_f between 2 and 10. The minimum loss time is thus still longer than the flow time

but not by a large factor, anymore; differences between the terrestrial and the Hermean magnetospheres with regard to the emptying of flux tubes should not be large in the magnetotail, but may become very significant as soon as one enters the dipolar field region where B_z increases and therefore the minimum loss time decreases.

VI. CHARGED PARTICLE ENVIRONMENT AT THE SURFACE OF MERCURY

In this section, we attempt to draw some inferences concerning the intensity of charged particles as a function of position on the surface of Mercury; this topic is of interest, among other reasons, because of possible effects of charged particle bombardment on surface material properties. Since two fly-bys provide only a very limited set of direct observations, we rely heavily on the previously discussed similarity of the magnetosphere of Mercury to a scaled-down terrestrial magnetosphere. Since Mercury is $S \approx 8$ times larger than the Earth in relation to the magnetosphere, a field line having invariant latitude Λ_E at the Earth corresponds, in the magnetospheric scaling, to a field line that intersects the surface of Mercury at a magnetic latitude Λ_M given by

$$\cos^2 \Lambda_M = S \cos^2 \Lambda_E$$

(to the extent that the field is dipolar out to a distance of S planetary radii, a reasonable approximation for our purposes). In what follows, all scaling of surface latitude values is obtained in this way.

We discuss separately the contributions from the solar wind and magnetosheath plasma, from the magnetospheric plasma sheet, and from galactic and solar cosmic rays.

Solar Wind Contribution - The magnetic field of Mercury is strong enough to stop the bulk motion of the solar wind before it reaches the planet's surface, most of the time. The average distance to the dayside magnetopause of 1.4 planetary radii is sufficiently small, however, so that infrequent temporary increases of the solar wind dynamic pressure to values sufficient to drive the solar wind flow into the planet are possible

(cf. Siscoe and Christopher, 1975). For example, a solar wind proton number density of 165 cm^{-3} together with a speed of 1000 km sec^{-1} would provide a sufficiently large dynamic pressure. Such enormous solar wind enhancements are very rare; however, the August 1972 event may have been such an enhancement.

During normal conditions, when the planetary magnetic field is able to hold off the solar wind pressure, access of magnetosheath plasma to the planet's surface may be possible along magnetic field lines. In the Earth's magnetosphere, magnetosheath plasma penetration occurs at the magnetospheric clefts (or dayside polar cusps), which reach down to the ionosphere at invariant latitudes typically 76-78° on the noon meridian. Neither Mercury I nor Mercury III trajectories crossed the corresponding region of the Hermean magnetosphere, so Mariner 10 did not provide any observations that would confirm or deny the existence of a magnetospheric cleft at Mercury. In view of the strong similarity between the terrestrial and the Hermean magnetospheres in many other observed aspects, we consider the existence of magnetospheric clefts at Mercury to be quite probable. The terrestrial cleft location from, say, 76° - 78° latitude at local noon scales to 50° - 57° on Mercury. The extent in local time should be the same as on the Earth, i.e., 4 to 6 hours on either side of local noon.

Plasma Sheet Contribution - As already discussed, Mariner 10 observed an electron plasma sheet at Mercury that appears to have similar properties and configuration to the plasma sheet in the Earth's magnetotail. The high-latitude boundary of the terrestrial plasma sheet of $Z_{SM} \approx 3\ R_E$ corresponds to an invariant latitude of about 72° on the midnight meridian (cf., e.g., Figure 6 of Fairfield, 1968). This scales to 35° at Mercury.

The low-latitude boundary requires a more detailed discussion, since it was not penetrated by Mariner 10. It may be the result of one or more effects: (a) emptying of flux tubes by precipitation (Kennel, 1969), (b) balance between convective flow and gradient-curvature drifts (Alfvén layer formation) (Kavanagh et al., 1968), (c) balance between convection and corotation electric fields (see Siscoe and Christopher, 1975, and references therein). In the Earth's magnetosphere, all these effects predict roughly the same location for the low-latitude boundary, consistent with the observed location of approximately 68° at midnight (during relatively quiet geomagnetic conditions). However, as discussed in Section V, none of these three effects scales from the Earth to Mercury: effect (c) is negligible (i.e., it alone would yield no significant low-latitude boundary), while (a) is considerably more important than at the Earth and predicts a boundary at approximately an equatorial distance equal to that of the dayside magnetopause, i.e., 1.4 R_M. At the Earth this would correspond to 11 R_E and an ionospheric latitude of 70° at midnight; this then scales to 25° at Mercury. Effect (b), if strong pitch-angle diffusion were operative in the Hermean plasma sheet, would produce a comparable low-latitude boundary location.

In short, the electron plasma sheet in the magnetotail of Mercury is expected to map down to a latitudinal band on each hemisphere of the surface of Mercury, whose boundaries on the midnight meridian are approximately 35° (determined by the thickness of the plasma sheet) and 25° (determined by the location of the Alfvén layer for plasma sheet electrons). We may speculate that, as in the case of the Earth, this band extends in local time toward the dayside and then connects to the magnetospheric cleft

expected to lie, on the average, from 50° to 57° on the noon meridian. The region of potential electron precipitation on the surface of Mercury is then rather similar to the auroral oval of the Earth--a narrow eccentric quasi-circular belt which reaches its highest latitude near local noon and its lowest latitude near local midnight. At Mercury, however, the belt lies at much lower latitudes and has a somewhat larger width than at the Earth. The intensity of the precipitation within this belt, as well as its possible variations with time and longitude, is at present entirely unknown: the intensity depends on precipitation-producing processes, such as particle-wave interactions, which are poorly known even in the case of the Earth and which are not expected to scale from one magnetosphere to the other.

Cosmic-Ray Contribution - At a given point on the surface of Mercury, particles with lower initial energies can reach the surface than at the corresponding point on the Earth, as a result of the lower magnetic dipole moment of Mercury. In the magnetic equatorial plane, where particle access is more restricted, protons with energies above 6.5 MeV can reach the surface from all directions; some directions are forbidden between 1.1 and 6.5 MeV, and only below 1.1 MeV are all directions forbidden. Thus, the magnetic field of Mercury offers essentially no shielding of the surface from galactic cosmic rays and from solar cosmic rays of more than a few MeV energy. As in the case of the Earth, we expect that the polar cap (the region lying poleward of the precipitation belt described above and threaded by field lines that presumably form the lobes of the magnetotail) should be accessible to solar cosmic rays of even lower energies.

VII. ATMOSPHERIC CONSIDERATIONS

Near closest approach during the Mercury III encounter, within the polar low flux region, the observed electron density was of the order of 0.1 cm^{-3}. This observation was made on an open magnetic flux tube (Ness et al., 1975) with one "foot" close enough to the terminator that a significant portion of the neutral atmosphere along the tube was in sunlight. Elsewhere in the magnetosphere the density was of the order of 1 cm^{-3}. In the following, we examine whether or not the observed electron densities could be of ionospheric origin. The neutral atmosphere is composed primarily of He (Broadfoot et al., 1974; Kumar, 1976), although some H was observed (Shemansky and Broadfoot, 1976). Thus, if the observed plasma is of ionospheric origin, it would be composed largely of He^+ ions and electrons.

Since the atmosphere is optically thin to ionizing radiations, the maximum ionospheric density on the dayside should be near the surface. The volume production rate for He^+ is $J\,[He]$, where $J = 3 \pm 2 \times 10^{-7}$ sec^{-1} is the photoionization rate and $[He]$ is the He density. Since electron recombination of He^+ is a very slow process, the major loss process for the ionosphere occurs at the surface where the plasma is absorbed. From the continuity equation, the loss rate for He^+ at the surface corresponds to the He^+ flow rate into the shadow which is of order $[He^+]\,V_{th}/H$, where $[He^+]$ is the He^+ density, V_{th} is the thermal speed of the ions and H is the He scale height, all quantities to be measured at the shadow point. Upon balancing the source and loss terms, we obtain $[He^+] \sim J\,[He]\,H/V_{th}$. We assume that the ion temperature near the foot of the flux tube is approximately the same as the neutral temperature of $\sim 100^{\circ}K$ (where a

low value has been selected to give the largest estimate for $[He^+]$), resulting in $V_{th} \simeq 7 \times 10^4$ cm sec^{-1} and $H \simeq 6 \times 10^6$ cm. These values together with the predicted He density $[He] \simeq 600$ cm^{-3} at 330 km (Hartle et al., 1975b) lead to the estimate $[He^+] \sim 1.6 \times 10^{-2}$ cm^{-3} for the maximum ionospheric density on the flux tube. This density is somewhat less than the observed electron density of 10^{-1} cm^{-3} near closest approach. Therefore, an atmospheric origin for the observed plasma within the polar low flux region is not probable, although it cannot be conclusively ruled out in view of the sizable observational and theoretical uncertainties. Within the plasma sheet regions, however, the electron density is of the order of 1 cm^{-3} while the predicted ionospheric density should be even less than 1.6×10^{-2} cm^{-3} since the feet of these flux tubes are mostly in darkness. We conclude, therefore, that the plasma observed in the Hermean magnetosphere (with the possible exception of that within the polar low flux region) is not of atmospheric origin but must have come from the solar wind.

VIII. MERCURY II OBSERVATIONS AND THEIR INTERPRETATION

We describe here observations made at the second encounter with the planet, Mercury II, which took place on September 21, 1974. The spacecraft passed at a distance of 50,000 km on the sunward side of the planet; the trajectory is shown in Figure 12 in solar ecliptic coordinates. The time of closest approach was 2059:00.82 seconds UT. As may be seen from the X_{SE}-Z_{SE} plot, the Z_{SE} coordinate varied between -5.3×10^4 km at 1900 and -0.85×10^4 km at 2300 UT. During this interval the spacecraft crossed the X_{SE} axis on the sunward side of Mercury and X_{SE} varied between 2.1×10^4 km at 1900 UT and 5.8×10^4 km at 2300 UT. This geometry is important for the interpretation of the observations to be presented below. The relevant data are shown in Figure 13 which covers the period to 2000 to 2300 UT. The upper panel shows the sum of the recorded counts in the highest energy channels, which is displayed rather than an integral over the corresponding energy interval in order to introduce no assumptions about the shape of the distribution function. The next panels show the counts from the 13.4 eV channel, the magnitude of the magnetic field $|F|$, the impact parameter R sin δ (see Figure 15) and the Y component of the impact parameter, considered as a vector from the center of the planet. Comparing this figure and Figure 12 we see that between 40 and 60 minutes after the time of closest approach, the data are different in character from that normally obtained when in the solar wind. We also see that the spacecraft position during this time is consistent with connection to the planet's vicinity by a field line not too different in orientation from the normal spiral direction. We note that the upper panel shows the higher energy electron fluxes to have been elevated

between 2150 and 2240 and that between 2200 and 2230 the interplanetary magnetic field magnitude was reduced.

We wish to consider the question, whether the data in Figure 14 constitutes evidence of the presence of a bow shock at Mercury, and if it does, whether we can deduce from it any information about the planetary interaction. In particular, we wish to know whether the fluctuations in the particle counting rates between 2150 and 2240 are due to the detection of electrons proceeding upstream from the shock along field lines connecting the spacecraft to the shock. It is known (Fairfield and Behannon, 1975) that low-frequency waves were observed in the magnetic field when Mariner 10 was situated on a field line connected to regions of the bow shock where there was a parallel alignment of field and shock normal. Upstream electron flux enhancements were observed, Figure 6, on both the inbound and outbound legs of the first encounter trajectory, and they are a relatively common occurrence at Earth and at Venus (Bridge et al., 1974). We therefore assume, Figure 15, that the most favorable situation for the observation of electron increases at Mercury II would have been when the impact parameter was small ($< 10\ R_p$) and directed towards the dawn side of the planet. The smaller the impact parameter, the less important the second condition becomes. Figure 15 does not illustrate the general case, as all vectors have been drawn in the plane, but it correctly illustrates the importance of the geometry. Referring back to Figure 14, we see that the enhanced flux region does generally coincide both with the region of depressed field, which could, however, merely indicate pressure balance in the solar wind, and with dawn connection. We have labeled the observed electron 'spikes' in Figure 12.

TABLE III

'Event'	R sin δ	Py	Relative Size	Remarks
A	5.7	- 2.5	1	Hit
B	4.0	+ 2.9	½	?Hit
C	15.7	- 8.3	2	Miss
D	25.8	-15.2	1	Miss
E	26.1	-10.8	½	Miss
F	15.6	+ 4.6	1½	Miss
G	3.8	- 0.6	1	Miss
A^1	3.7	+ 1.7	0	Hit
B^1	2.3	+ 1.5	0	Hit
C^1	4.4	- 2.6	0	Hit
D^1	6.1	- 5.1	0	Hit

In Figure 6, the spectra of upstream enhancements observed during the Mercury I encounter is compared with the spectrum of spike C, indicated in Figure 13. Both spectra indicate a relative enhancement of at least an order of magnitude between spike and typical solar wind spectra above $\sim$ 60 eV, and both have a similar convex form; this evidence of spectral form and intensity is consistent with a common origin for these spikes at Mercury I and Mercury II.

Turning to a detailed examination of the impact parameter and the connection point for seven individual electron enhancements, and for four low values of impact parameter which occurred without coincident electron increases, we refer to Table III. The last column of Table II indicates whether a straight line through the point of observation, and having the magnetic field direction at the time of observation, intersects a model of the bow shock of Mercury. This model is simply a scaled representation of the Earth's bow shock, described in Scudder et al. (1973). It does not seem to be possible to formulate a set of criteria which explain why event C is large, while for example, event C^1 is small. Since the instrument was turned off except for a few hours surrounding the time of closest approach, in order to conserve detector life-time, it has not been possible to make an exhaustive search for flux increases not associated with encounter. Field reductions, such as that observed between 2200 and 2230 are not unknown in the solar wind. During 58 days in the months of March and April 1974, for example, the magnetometer on Mariner 10 observed 17 examples of field magnitude reductions of greater than 50%, lasting more than 10 minutes (N. Ness, private communication).

In summary, the evidence for the experiment having detected the presence of Mercury's bow shock at the second encounter is inconclusive. Mercury's bow shock has a radius of $\sim 4\ R_m$ and there are times, Figure 15, when $R \sin \delta < 5\ R_m$ and no electron increase is observed. The absence of flux increases before 2140 or after 2240, the partial correspondence of the times of increase of some events with the magnitude and sign of the impact parameter, and the spectrum of the "spikes", support the relation of these events to Mercury's bow shock, and make it likely that, at the time of Mercury II, the planet's interaction with the solar wind was characterized by the presence of a bow shock similar to that observed at Mercury I and at Mercury II. However, the fact that the largest increases occurred at times when the magnetic field did not make a rectilinear connection to the bow shock make it impossible to state this conclusion with certainity.

IX. SUMMARY

The two night-side encounters with Mercury's magnetosphere by Mariner 10 (Mercury I and III) relealed bow shock and magnetosheath signatures in the plasma electron data that are entirely consistent with the geometry expected for an interaction between a planet centered magnetic dipole and the solar wind.

The geometrically determined distance between the planet's center and the solar wind stagnation point is 1.4 ± 0.1 planetary radii (R_M), which is in satisfactory agreement with the value expected for a dipole with the strength determined by the magnetometer experiment.

Both diffuse and sharp shock crossings were observed on the two magnetosphere encounters. The difference is interpreted in terms of the change in character expected for different orientations of the magnetic field relative to the shock normal.

Electron intensity increases ('spikes') upstream from the bow shock were observed on the first Mercury encounter. They appeared in association with the diffuse (pulsating) portion of the shock. They are very similar both qualitatively and quantitatively to electron spikes observed upstream from the Earth's bow shock. Events of a similar kind were observed further upstream on the second Mercury encounter, but the implied identification should be regarded as highly suggestive rather than conclusive.

The magnetospheric scaling implied by the fit of the Earth's bow shock and magnetopause to the Mercury encounter data can be expressed quantitatively by the relation

$$L_E = (8 \pm 0.5)\, L_M$$

where L is distance normalized to the respective planetary radii, Earth (E) and Mercury (M). This conversion factor is slightly larger than had been derived from the preliminary analysis of the Mercury encounter data.

The interior plasma features of Mercury's magnetosphere are very similar to a scaled down version of those of Earth's magnetosphere with approximately the same scaling factor given above. The specific features used to make this generalization were the cool plasma sheet, the hot plasma sheet, and the polar low flux region.

The energies of the plasma sheet electrons at Mercury are essentially the same as those in the plasma sheet at Earth. The plasma sheet number densities at Mercury are increased relative to those at Earth in approximately the same ratio as the solar wind number density. Time intervals should scale by being reduced at Mercury a factor of about 20 compared to Earth; substorm time scales then become on the order of a few minutes at Mercury.

Magnetospheric features and processes that do not scale simply from Earth to Mercury include: the plasmasphere and trapped radiation belts, both of which are precluded by the large size of the planet relative to its magnetosphere; ionospheric effects on magnetospheric motions should be absent; particle gyroradii do not scale as the size of the magnetosphere with the result that the inner edge of the plasma sheet (which is a finite gyroradius effect) at Mercury lies relatively farther out in the magnetosphere, in terms of Earth's magnetosphere, it lies at 10 R_E instead of the actual value for Earth which is about 7 R_E; the particle loss cone at Mercury is larger than the value at the corresponding place in Earth's magnetosphere, and consequently particle loss processes are potentially more important there.

By extending the analogy with Earth's magnetosphere to include the dayside polar cleft, we would expect the surface of Mercury to be bombarded by solar wind particles in both hemispheres over a latitudinal range from 50° to 57° and extending east and west of local noon by 60° to 90°. Auroral precipitation onto the surface from the plasma sheet should occur in a latitudinal band from 25° to 35° at midnight and extend from there east and west with a poleward slant to merge with the dayside cleft. Occasional large solar storms should cause the solar wind to impact the entire dayside surface. The magnetic field of Mercury offers essentially no shielding of the surface from galactic cosmic rays and from solar cosmic rays of more than a few MeV energy.

The atmosphere of Mercury appears to have no significant magnetospheric effect, either through providing ionospheric closure of field aligned currents or through providing a source of low energy ions.

ACKNOWLEDGMENT

We would like to acknowledge extensive discussion of the results and interpretations given in this paper with our colleagues at MIT: H. S. Bridge, A. J. Lazarus, and S. Olbert; and with colleagues on the magnetometer team, N. F. Ness, K. W. Behannon and R. P. Lepping. We acknowledge the access we have had to magnetometer results prior to publication.

The experiment was carried out as a cooperative effort by scientists and engineers at the Boeing Company, the Goddard Space Flight Center, the Los Alamos Scientific Laboratory, and the Massachusetts Institute of Technology. Although we cannot acknowledge by name all of the individuals whose efforts were essential to the success of this experiment, we would like to express our deep appreciation of their contributions to this work, especially those of H. S. Bridge, S. J. Bame, and R. Butler.

REFERENCES

Armstrong, T. P., S. M. Krimigis, L. J. Lanzerotti, "A reinterpretation of the reported energetic particle fluxes in the vicinity of Mercury", J. Geophys. Res., 80, 4015, 1975.

Bridge, H. S., A. J. Lazarus, K. W. Ogilvie, J. D. Scudder, R. E. Hartle, J. R. Asbridge, S. J. Bame, W. C. Feldman, G. L. Siscoe, C. M. Yeates, "Preliminary report of results from the plasma science experiment on Mariner 10", Space Research XV, pp. 501-519, Akademie-Verlag, Berlin, 1975.

Broadfoot, A. L., S. Kumar, M. J. S. Belton, M. B. McElroy, "Mercury's atmosphere from Mariner 10: preliminary results", Science, 185, 166, 1975.

Choe, J. T., D. B. Beard, E. C. Sullivan, "Precise calculation of the magnetosphere surface for a tilted dipole", Planet. Space Sci., 21, 485, 1973.

Christon, S. P., S. F. Daly, J. H. Eraker, M. A. Perkins, J. A. Simpson, A. J. Tuzzolino, "Response of instrumentation on Mariner 10 for low energy, high intensity particle measurements in Mercury's magnetosphere", preprint 1976.

DeForest, S. F., C. E. McIlwain, "Plasma clouds in the magnetosphere", J. Geophys. Res., 76, 3587, 1971.

Fairfield, D. H., "Magnetospheric field configuration", J. Geophys. Res., 73, 7329, 1968.

Fairfield, D. H., "Average and unusual locations of the earth's magnetopause and bow shock", J. Geophys. Res., 76, 6700, 1971.

Fairfield, D. H. and K. W. Behannon, "Bow shock and magnetosheath waves at Mercury", J. Geophys. Res., 81, , 1976.

Frank, L. A., "Magnetospheric and auroral plasma", Rev. of Geophysics and Space Physics, 13, 974, 1975.

Gonzalez, W. D., F. S. Mozer, "A quantitative model for the potential resulting from reconnection with an arbitrary interplanetary magnetic field", J. Geophys. Res., 79, 4186, 1974.

Greenstadt, E. W., "Observations of nonuniform structure of the Earth's bow shock correlated with interplanetary field orientation", J. Geophys. Res., 77, 1729, 1972a.

Greenstadt, E. W., "Binary index for assessing local bow shock obliquity", J. Geophys. Res., 77, 5467, 1972b.

Hartle, R. E., S. A. Curtis, G. E. Thomas, "Mercury helium exosphere", J. Geophys. Res., 80, 3689, 1975b.

Hartle, R. E., K. W. Ogilvie, J. D. Scudder, H. S. Bridge, G. L. Siscoe, A. J. Lazarus, V. M. Vasyliunas, C. M. Yeates, "Preliminary interpretation of plasma electron observations at the third encounter of Mariner 10 with Mercury", Nature, 255, 206, 1975.

Howard, H. T., G. L. Tyler, P. B. Esposito, J. D. Anderson, R. D. Rosenberg, I. I. Shapiro, C. Fjeldbo, A. J. Kliore, G. S. Levy, D. L. Brunn, R. Dickerson, R. E. Edelson, W. L. Martin, R. B. Postal, B. Seidel, T. T. Sesplaukis, D. L. Shinley, C. T. Stelzried, D. N. Sweetnam, G. E. Wood, A. J. Zygielbaum, "Mercury: results on mass, radius, ionosphere, and atmosphere from Mariner-10 dual-frequency radio signals", Science, 185, 182, 1974.

Howe, H. C., Jr., J. H. Binsack, "Explorer 33 and 35 plasma observations of magnetosheath flow", J. Geophys. Res., 77, 3334, 1972.

Kavanagh, L. D., Jr., J. W. Freeman, A. J. Chen, "Plasma flow in the magnetosphere, J. Geophys. Res., 73, 5511, 1968.

Kennel, C. F., "Consequences of a magnetospheric plasma", Rev. Geophys. 7, 379, 1969.

Konradi, A., D. J. Williams, T. A. Fritz, "Observations of proton spectra ($1.0 \leq E_p \leq 300$ keV) and fluxes at the plasma pause", J. Geophys. Res., 78, 4739, 1973.

Kumar, S., "Mercury's atmosphere: a perspective after Mariner 10", Icarus, in press, 1976.

Montgomery, M. D., J. R. Asbridge, S. J. Bame, "Vela 4 plasma observations near the earth's bow shock", J. Geophys. Res., 75, 1217, 1970.

Montgomery, M. D., J. R. Asbridge, S. J. Bame, E. W. Hones, "Low-energy electron measurements and spacecraft potential: Vela 5 and Vela 6", "Photon and particle interactions with surfaces in space", R. J. L. Grard ed., Reidel, Dordrecht, 1973.

Ness, N. F., K. W. Behannon, R. P. Lepping, Y. C. Whang, K. H. Schatten, "Magnetic field observations near Mercury: preliminary results from Mariner 10, Science, 185, 150, 1974.

Ness, N. F., K. W. Behannon, R. P. Lepping, Y. C. Whang, "Interaction of solar wind with Mercury and its magnetic field", Proc. Bilateral Seminar, Moscow, USSR, NASA SP-397, and "Observations of Mercury's Magnetic Field", Icarus, 28, 479, 1975b.

Ness, N. F., K. W. Behannon, R. P. Lepping, Y. C. Whang, "The magnetic field of Mercury-I", J. Geophys. Res., 80, 2708, 1975a.

Ness, N. F., "The magnetic field of Mercury", Proceedings of General Assembly IAU, Grenoble, 1976.

Ogilvie, K. W., J. D. Scudder, R. E. Hartle, G. L. Siscoe, H. S. Bridge, A. J. Lazarus, J. R. Asbridge, S. J. Bame, C. M. Yeates, "Observations at Mercury encounter by the plasma science experiment on Mariner 10", Science, 185, 143, 1974.

Scudder, J. D., D. L. Lind, K. W. Ogilvie, "Electron observations in the solar wind and magnetosheath", J. Geophys. Res., 78, 6535, 1973.

Scudder, J. D., "Determination of solar wind bulk speeds from Mariner 10 electron observations", J. Geophys. Res., , , 1976.

Shemansky, D. E., A. L. Broadfoot, "Mariner 10 U.V. experiment: hydrogen on Mercury", EOS, 57, 279, 1976.

Simpson, J. A., J. H. Eraker, J. E. Lamport, P. H. Walpole, "Electrons and protons accelerated in Mercury's magnetic field", Science, 185, 160, 1974.

Siscoe, G. L. and L. Christopher, "Variations in the solar wind stand-off distance at Mercury", Geophys. Res. Letters, 2, 158, 1975.

Siscoe, G. L., N. F. Ness, C. M. Yeates, "Substorms on Mercury?", J. Geophys. Res., 80, 4359, 1975.

Smith, P. H., R. A. Hoffman, "Ring current particle distributions during the magnetic storms of December 16-18, 1971", J. Geophys. Res., 78, 4731, 1973.

Sonnerup, B. U. Ö., "Magnetopause reconnection rate", J. Geophys. Res., 79, 1546, 1974a.

Sonnerup, B. U. Ö., "The reconnecting magnetosphere", "Magnetospheric Physics", B. M. McCormac, ed., D. Reidel, Dordrecht, 1974, pp. 23-33.

Vasyliunas, V. M., "Magnetospheric Plasma", "Solar Terrestrial Physics - 1970" pt. 3, p. 192, E. R. Dyer ed., D. Reidel, Dordrecht, 1972.

Vasyliunas, V. M., Paper presented at AGU annual meeting 1974.

Vasyliunas, V. M., "Theoretical models of magnetic field line merging, 1", Rev. Geophysics and Space Physics, 13, 303, 1975a.

Vasyliunas, V. M., "Concepts of magnetospheric convection", "The Magnetospheres of the Earth and Jupiter", V. Formisano, ed., D. Reidel, Dordrecht, 1975b, pp. 179-188.

Wolf, R. A., "Ionosphere-magnetosphere coupling", Space Sci. Reviews, 17, 537, 1975.

FIGURE CAPTIONS

Figure 1 The trajectory of Mariner-10 viewed from the north ecliptic pole. Mercury makes two orbits during the orbital period of Mariner 10.

Figure 2 Encounter trajectories at Mercury I and Mercury III, viewed from the north ecliptic pole and the solar direction.

Figure 3 a). The ion and electron instrument fields of view and arrangement on the scan platform. b). An exploded drawing of the electron spectrometer. Note details of the channeltrons and slits. c). Scanning angles for forward and backward detectors.

Figure 4 Combined energetic particle, magnetic field, and plasma observations obtained at Mercury I. BS - bow shock, MP - magnetopause, CA - closest approach.

Figure 5 Electron spectra obtained in the solar wind, the magnetosheath, and for upstream electron spikes observed at Mercury I and Mercury III.

Figure 6 Combined magnetic field and plasma observations obtained at Mercury III.

Figure 7 The trajectories at Mercury I and Mercury III seen from the solar direction. The magnetic equator found by Ness et al., 1975 is added, and the plasma electron characteristics are shown at corresponding points along the orbit. The trace of the magnetosphere is shown approximately and the shaded region represents the projection of the plasma sheet.

Figure 8 Three electron spectra. On the left a "cool plasma sheet" spectrum from Mercury III. The high flux at low energies is photoelectrons and shows the effect of spacecraft charging. The shaded region is a scaled photoelectron spectrum from IMP-6. The center spectrum is a "cool plasma sheet" spectrum from Mercury I, and the right is a "hot plasma sheet" spectrum from Mercury I.

Figure 9 The solid curves are best fits to average locations of the magnetopause and bow shock from Fairfield (1971). The dotted lines are fits to the plasma observations of Howe and Binsack (1972). The data points represent the boundary positions observed at Mercury by Mariner-10 multiplied by 7 (dots), 8 (crosses) and 9 (triangles).

Figure 10 A comparison between magnetic field observations at Earth by Fairfield and at Mercury by Ness. The subsolar stagnation points have been scaled to coincide.

Figure 11 Spectra, in units of particles/cm^2/sec/sterad/keV, from corresponding regions of Mercury and the Earth. IMP-6 data by courtesy of E. F. Hones.

Figure 12 The trajectory of Mariner-10 around the time of the second Mercury encounter. An approximate bow shock and intersecting lines from a representative spacecraft position have been added to illustrate the requirements for intersection of the interplanetary field with the bow shock.

Figure 13 Data obtained at Mercury II; top, the sum of the highest energy channel counting rates and the counting rate of the 13.4 eV channel; below, the magnetic field magnitude, the impact parameter and its component in the Y_{SE} direction.

Figure 14 A diagram showing shock-intersection geometry for the special case of a magnetic field line in the trajectory-planet plane.

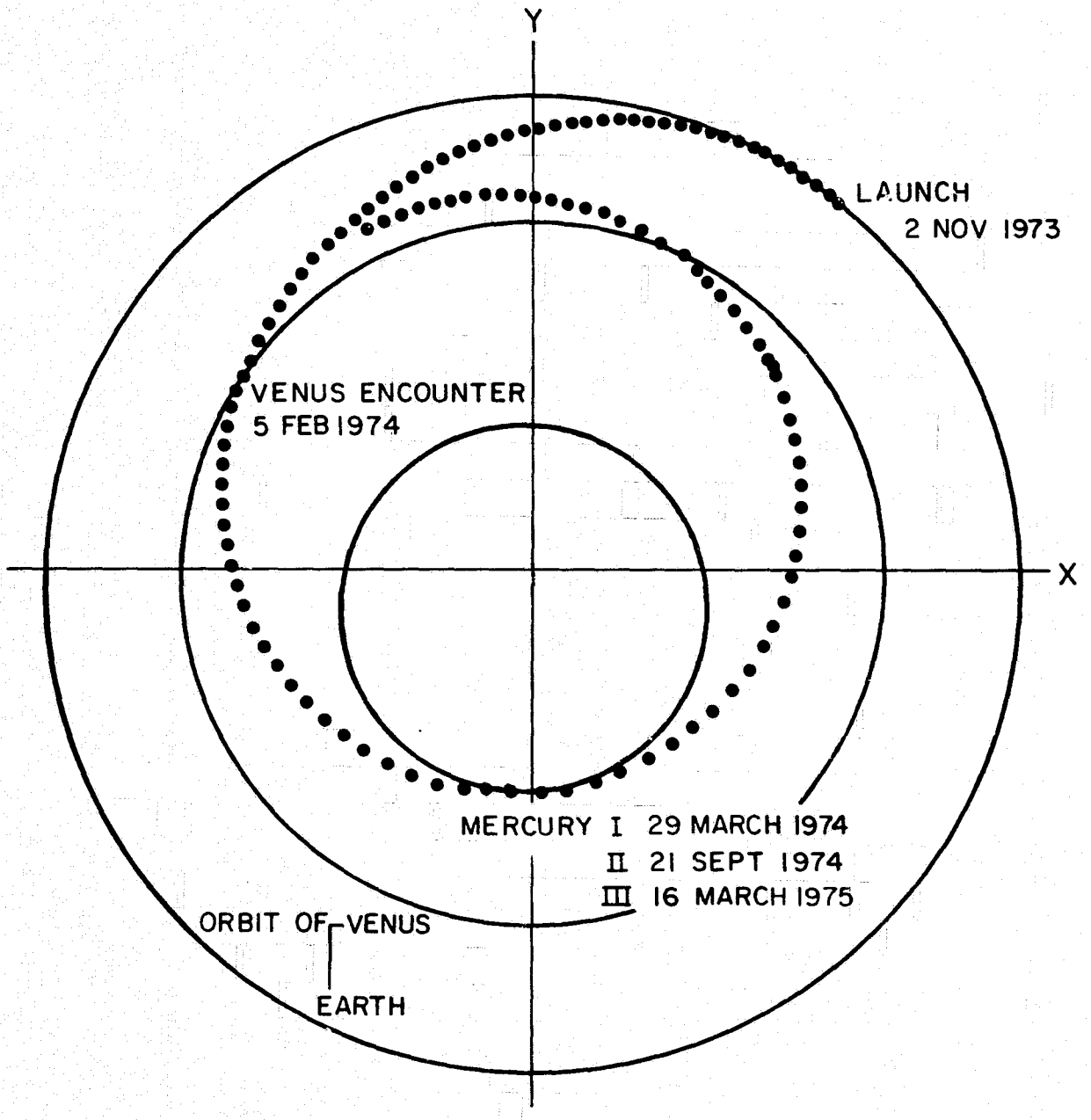
Y
X
LAUNCH
2 NOV 1973
VENUS ENCOUNTER
5 FEB 1974
MERCURY I 29 MARCH 1974
II 21 SEPT 1974
III 16 MARCH 1975
ORBIT OF VENUS
EARTH

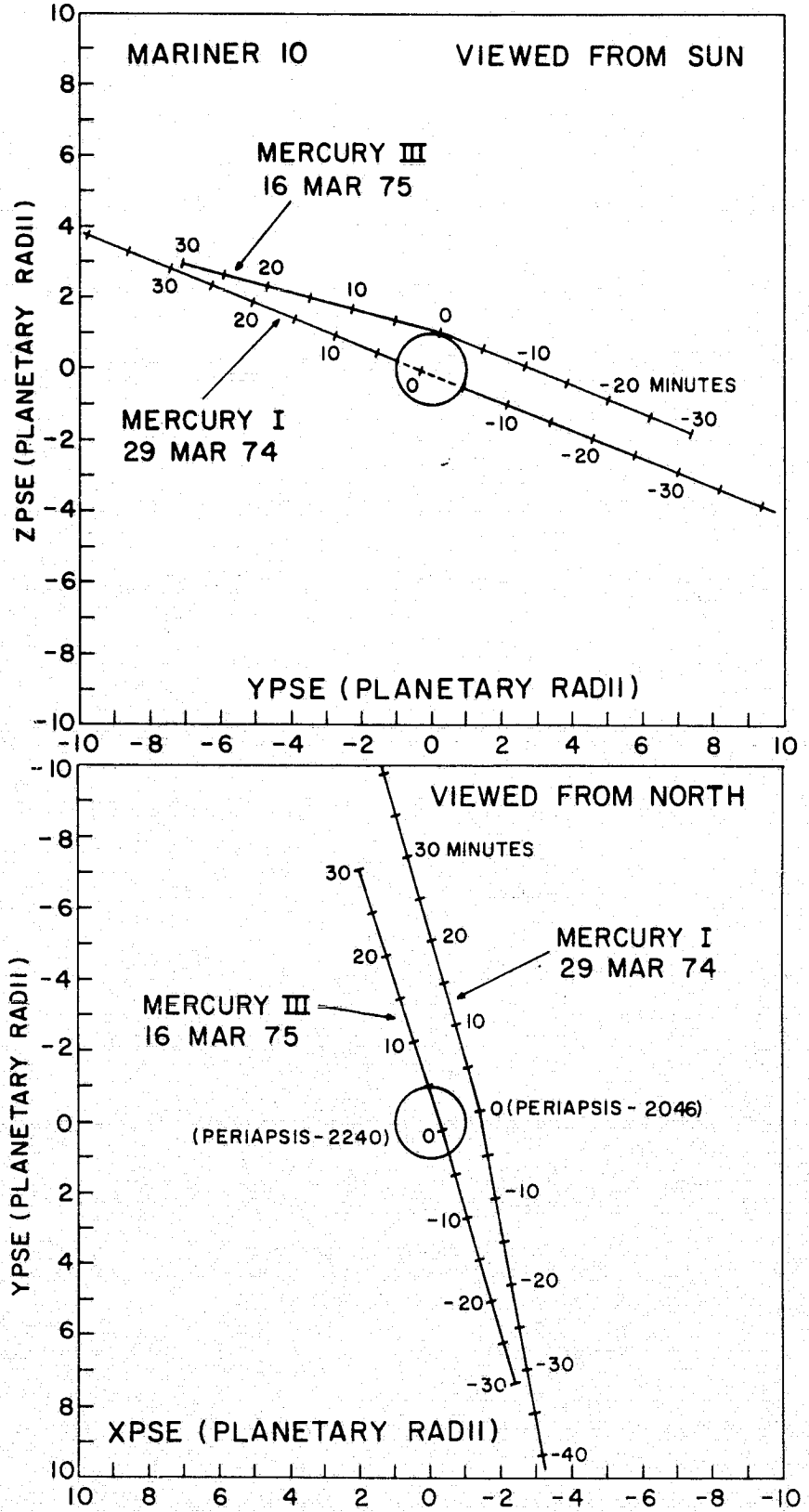
MARINER 10
VIEWED FROM SUN
MERCURY III
16 MAR 75
MERCURY I
29 MAR 74
-20 MINUTES
ZPSE (PLANETARY RADII)
YPSE (PLANETARY RADII)
VIEWED FROM NORTH
30 MINUTES
MERCURY I
29 MAR 74
MERCURY III
16 MAR 75
0 (PERIAPSIS - 2046)
(PERIAPSIS - 2240)
YPSE (PLANETARY RADII)
XPSE (PLANETARY RADII)

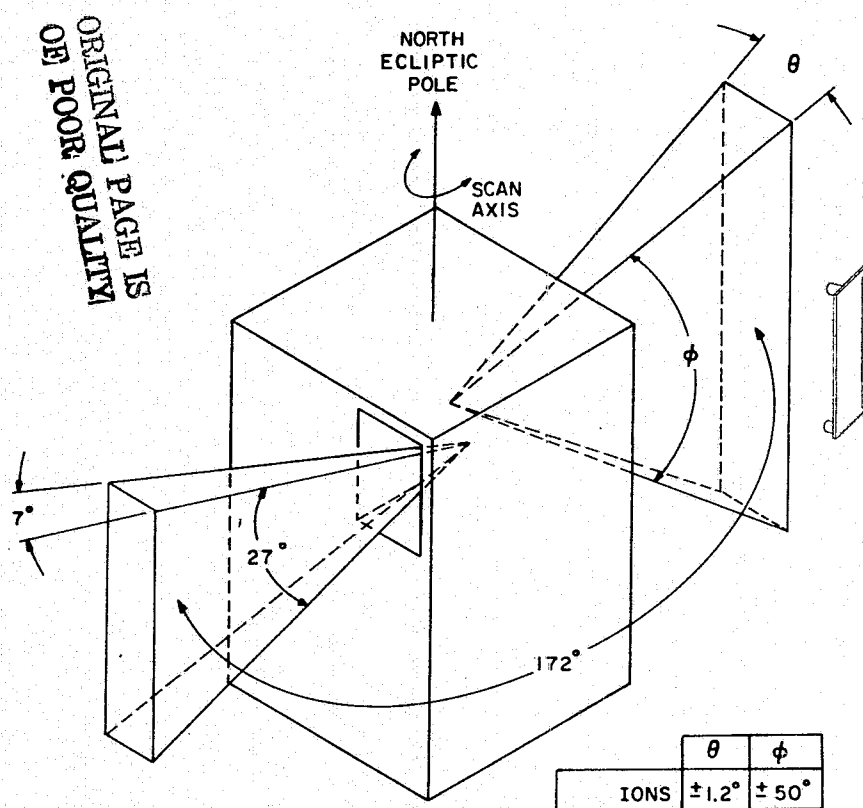

	θ	φ
IONS	±1.2°	±50°
ELECTRONS	±2.9°	±64°

(a)

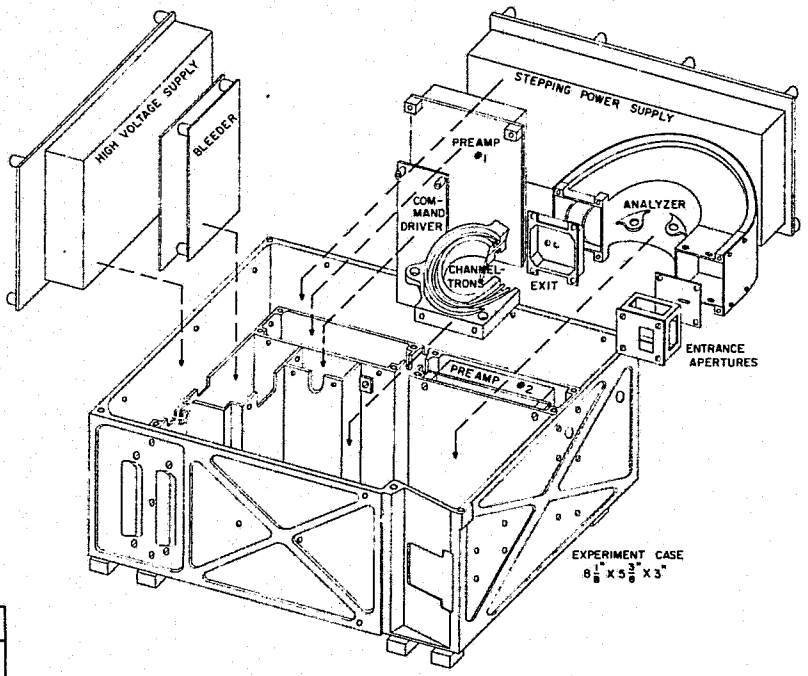

(b)

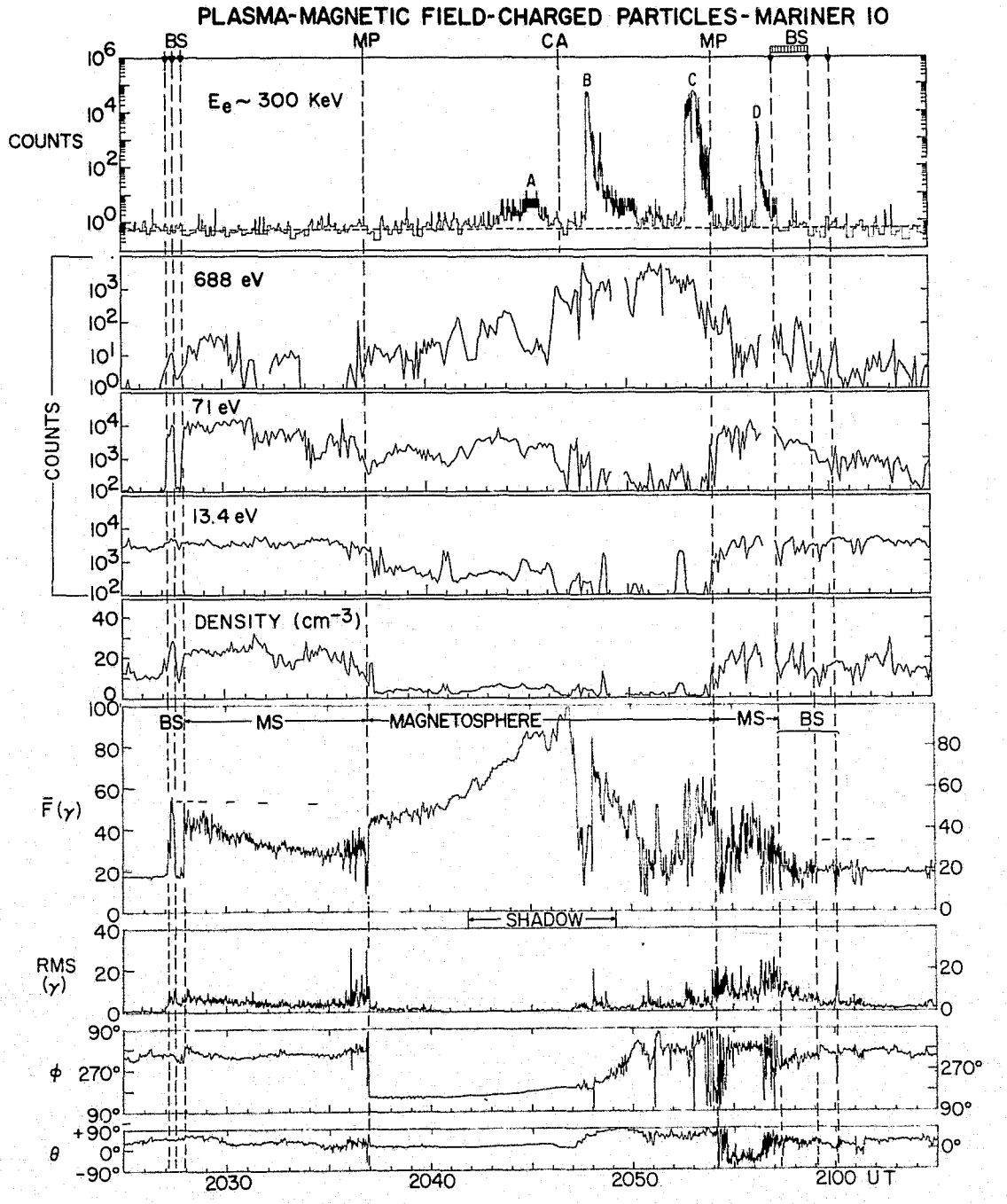

29 MARCH 1974

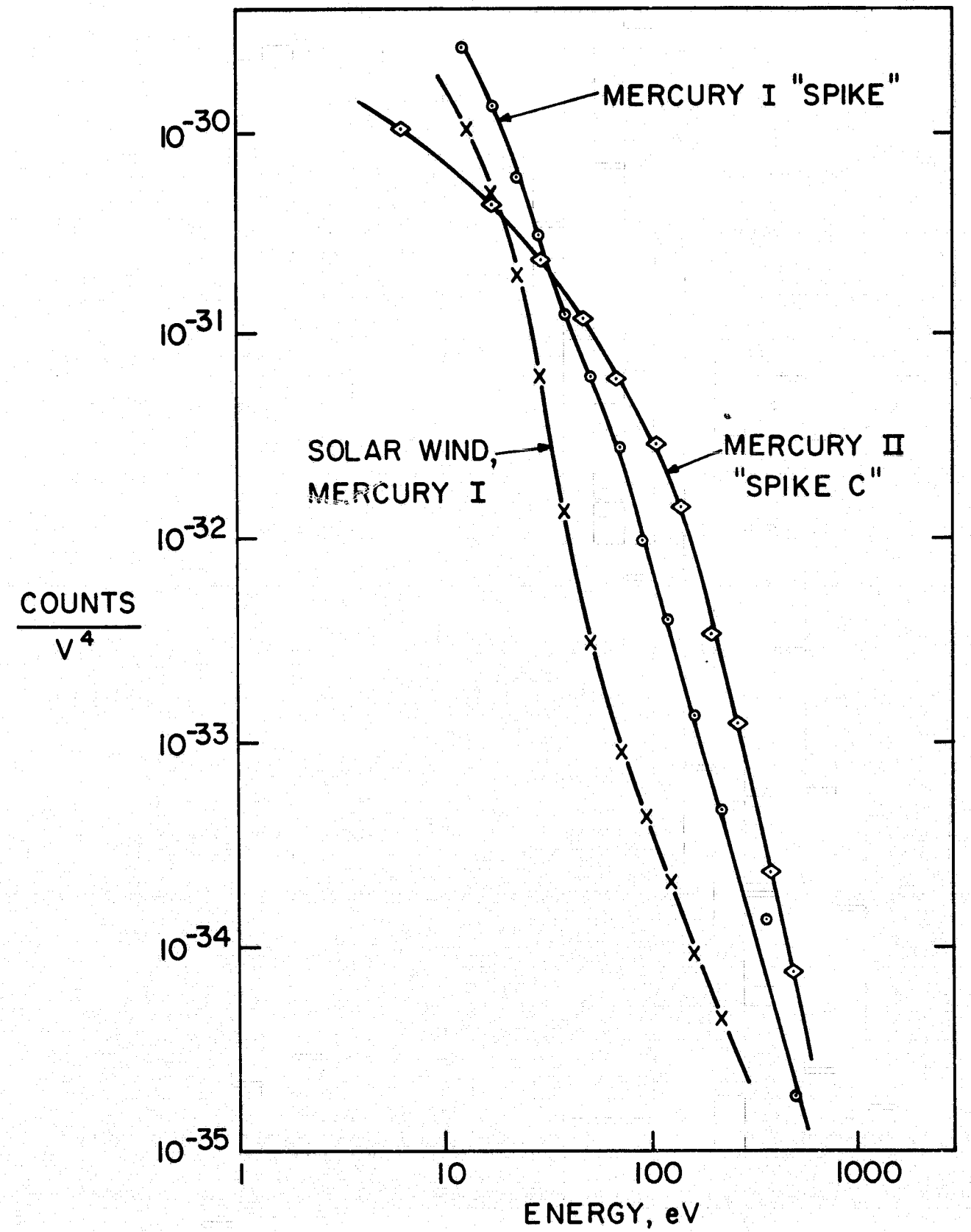
MERCURY I "SPIKE"
SOLAR WIND,
MERCURY I
MERCURY II
"SPIKE C"
COUNTS
V⁴
10⁻³⁰
10⁻³¹
10⁻³²
10⁻³³
10⁻³⁴
10⁻³⁵
1
10
100
1000
ENERGY, eV

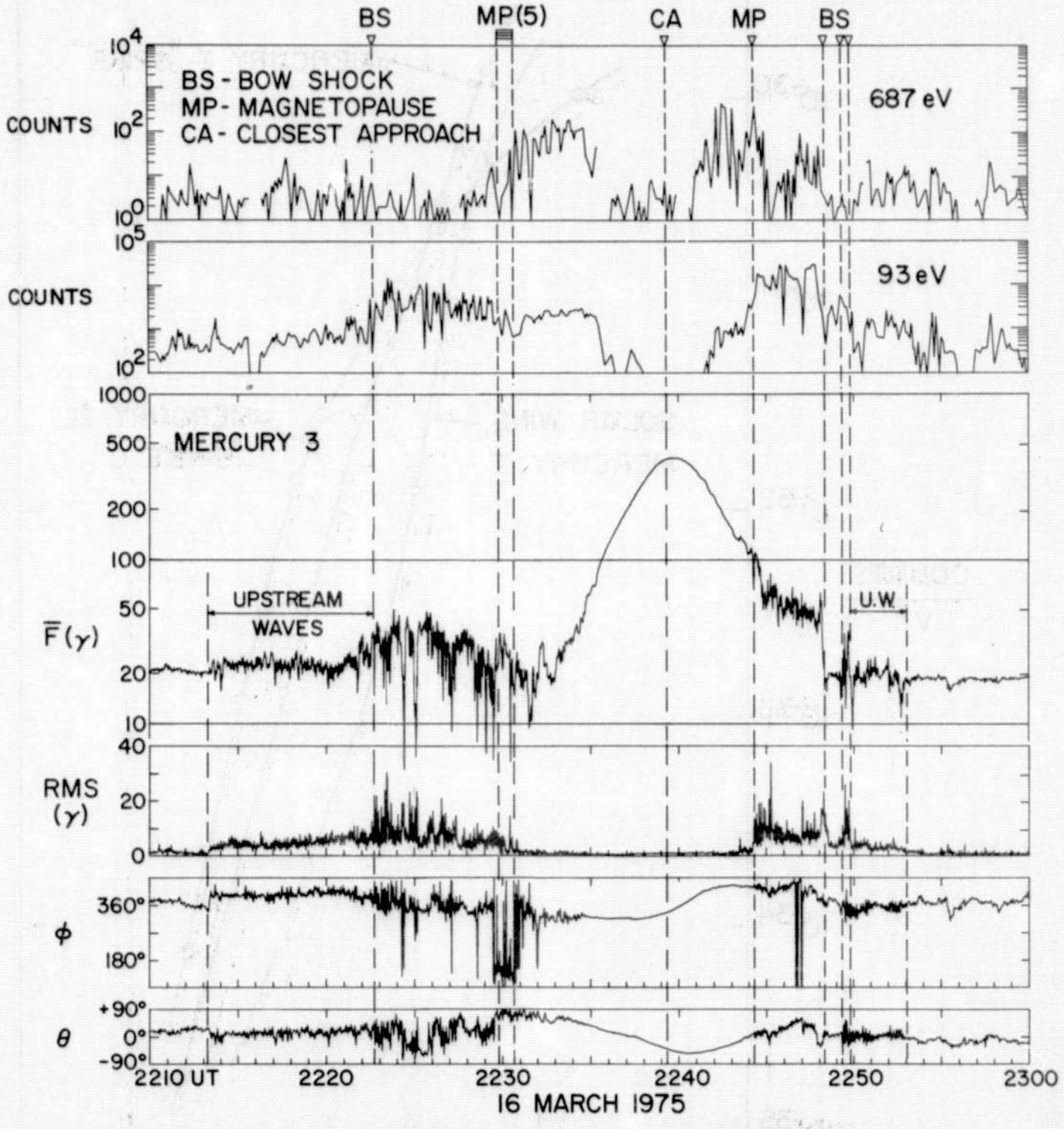
BS
MP(5)
CA
MP
BS
BS - BOW SHOCK
MP - MAGNETOPAUSE
CA - CLOSEST APPROACH
687 eV
93 eV
COUNTS
COUNTS
MERCURY 3
UPSTREAM
WAVES
U.W
F̄(γ)
RMS
(γ)
φ
θ
2210 UT
2220
2230
2240
2250
2300
16 MARCH 1975

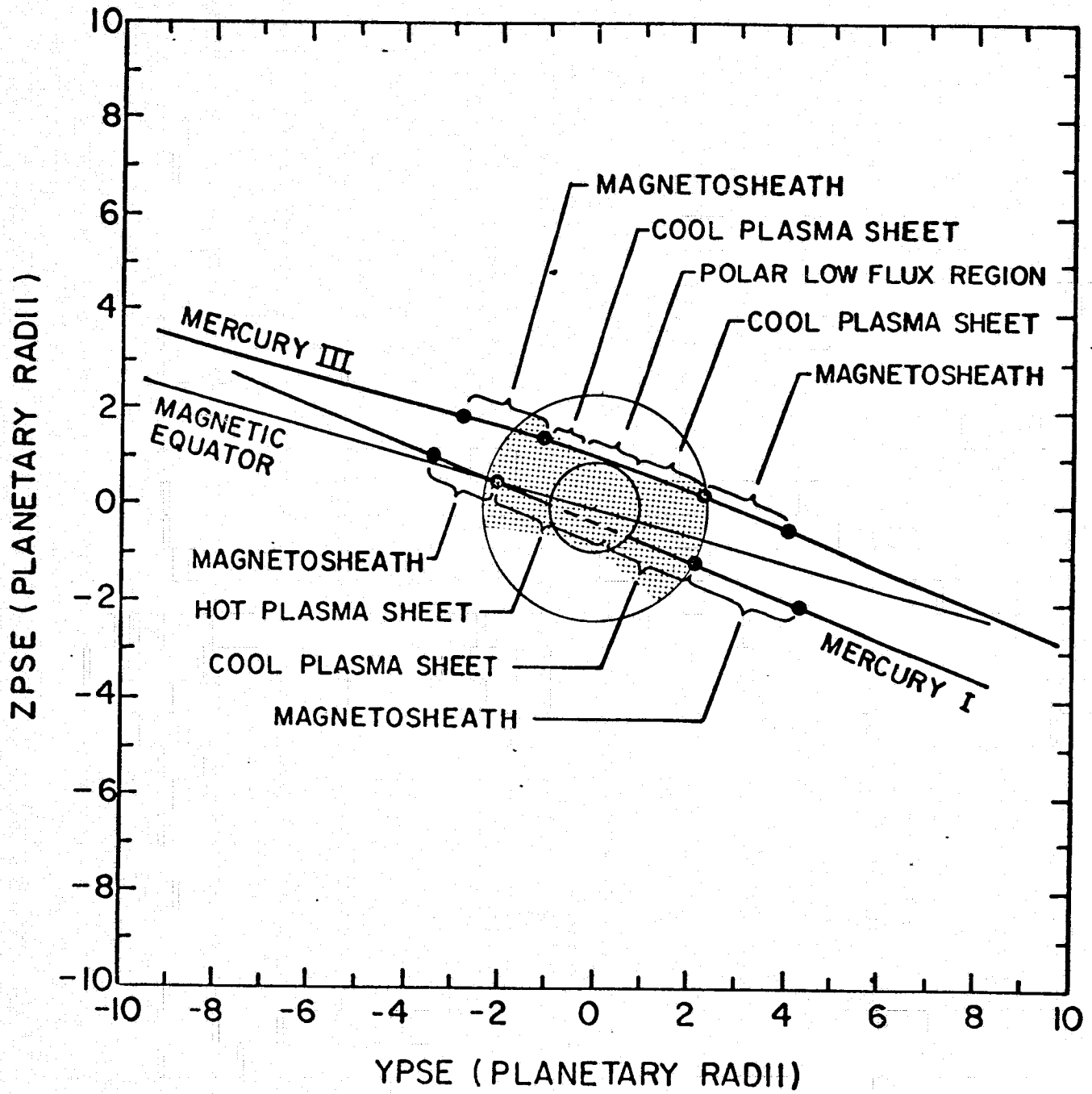
MAGNETOSHEATH
COOL PLASMA SHEET
POLAR LOW FLUX REGION
COOL PLASMA SHEET
MAGNETOSHEATH
MERCURY III
MAGNETIC EQUATOR
MAGNETOSHEATH
HOT PLASMA SHEET
COOL PLASMA SHEET
MAGNETOSHEATH
MERCURY I
ZPSE (PLANETARY RADII)
YPSE (PLANETARY RADII)
10
8
6
4
2
0
-2
-4
-6
-8
-10
-10 -8 -6 -4 -2 0 2 4 6 8 10

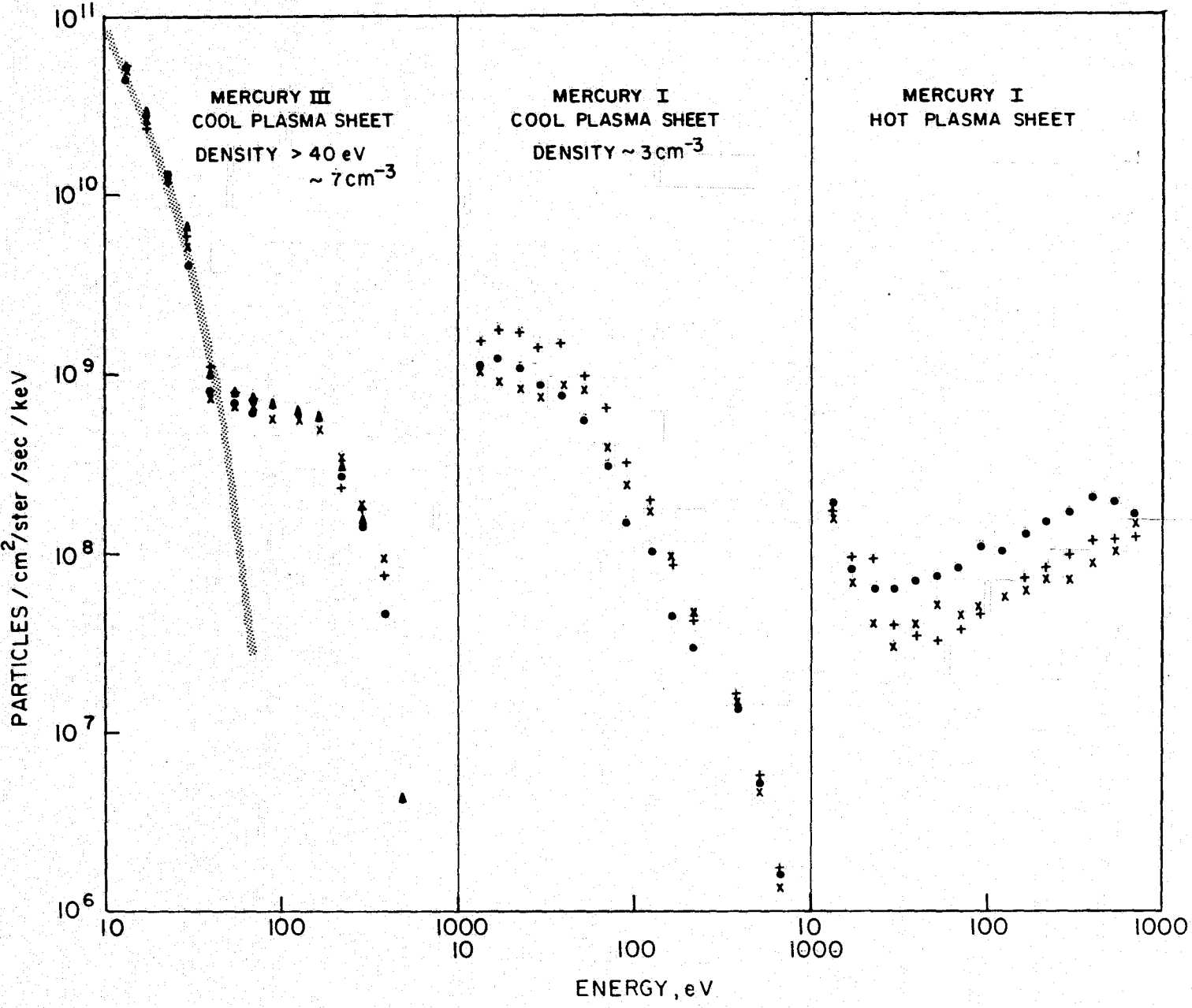
MERCURY III
COOL PLASMA SHEET
DENSITY > 40 eV
~ 7 cm⁻³
MERCURY I
COOL PLASMA SHEET
DENSITY ~ 3 cm⁻³
MERCURY I
HOT PLASMA SHEET
PARTICLES / cm² / ster / sec / keV
ENERGY, eV
10¹¹
10¹⁰
10⁹
10⁸
10⁷
10⁶
10
100
1000
10
100
1000
10
100
1000

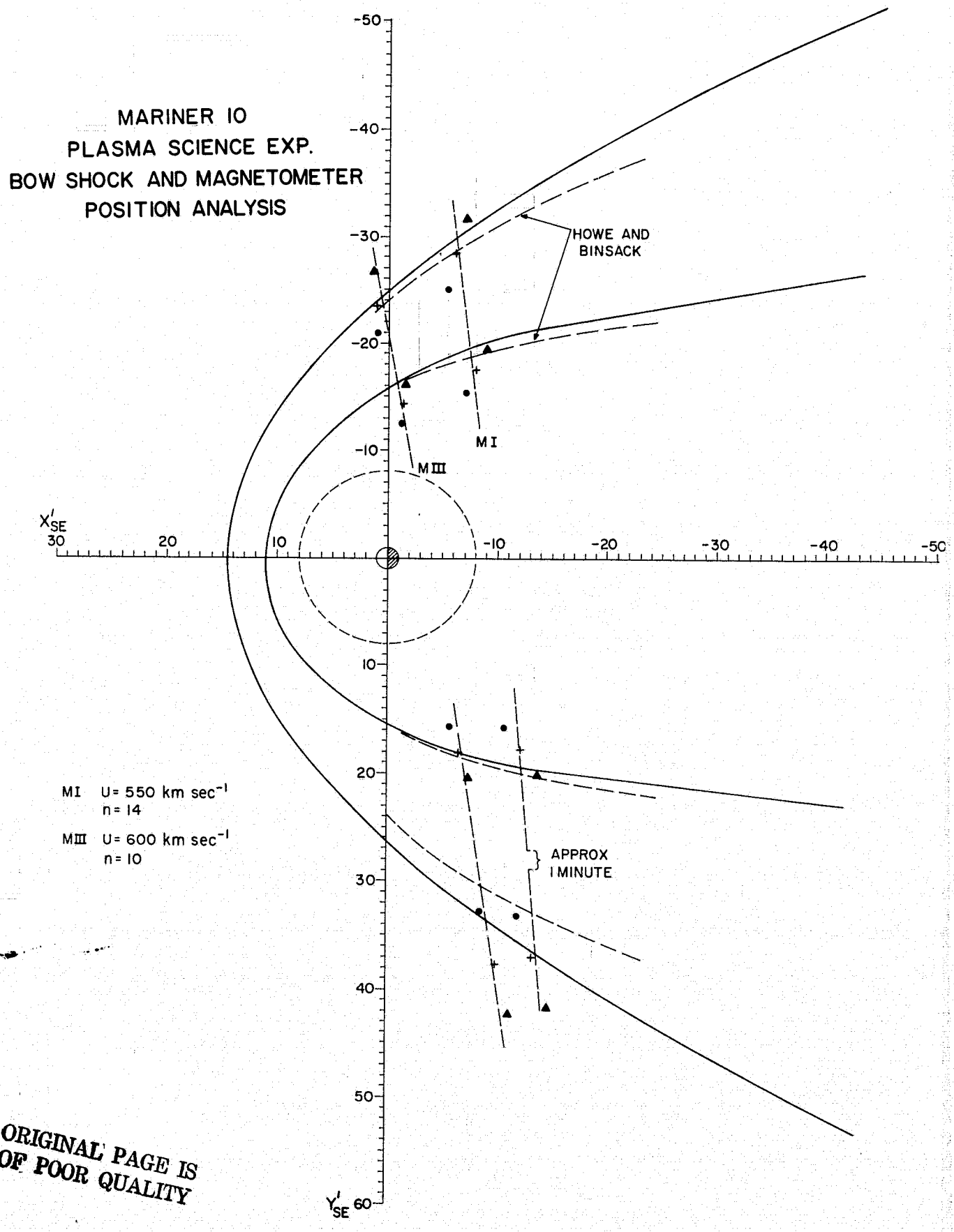

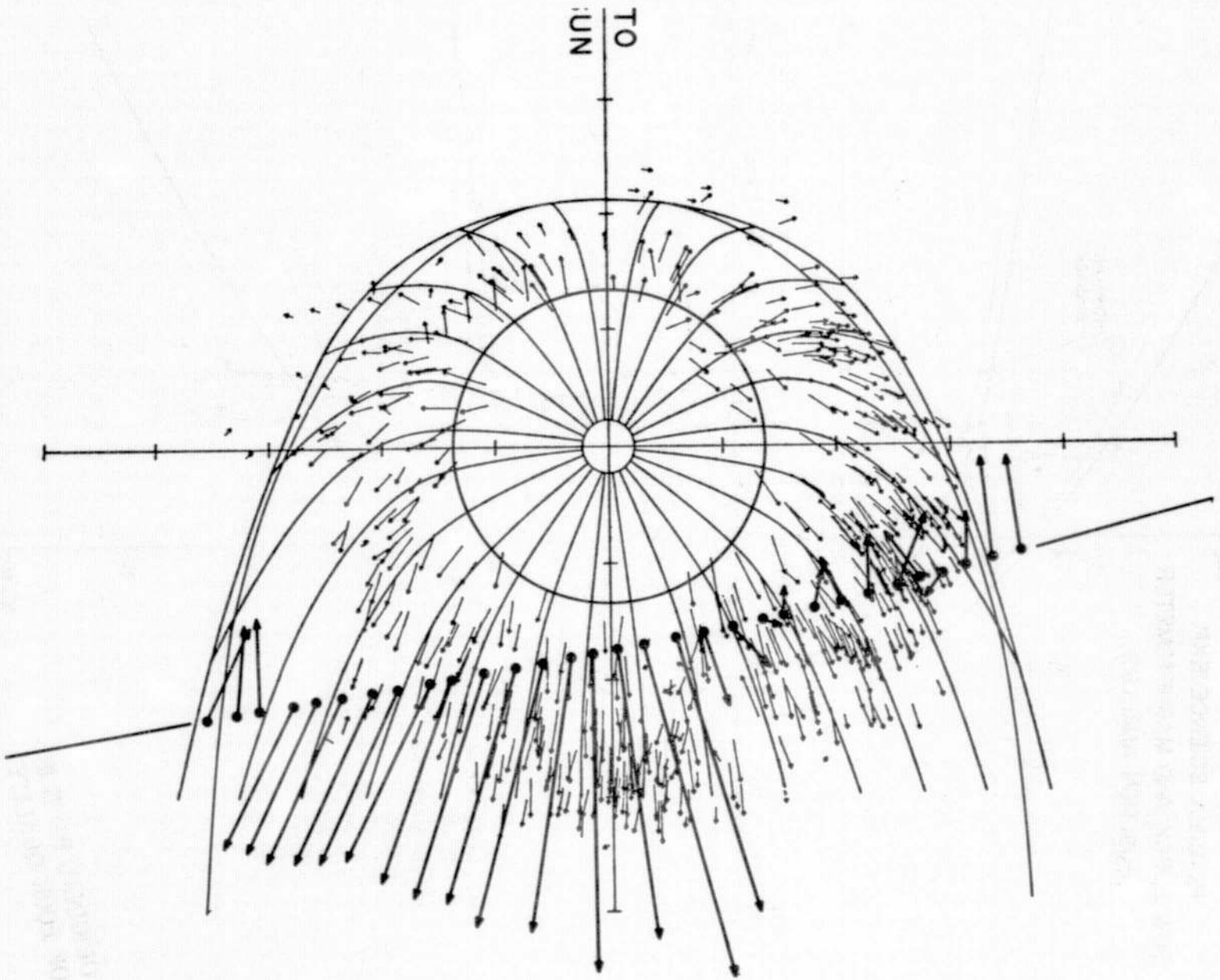
TO
SUN

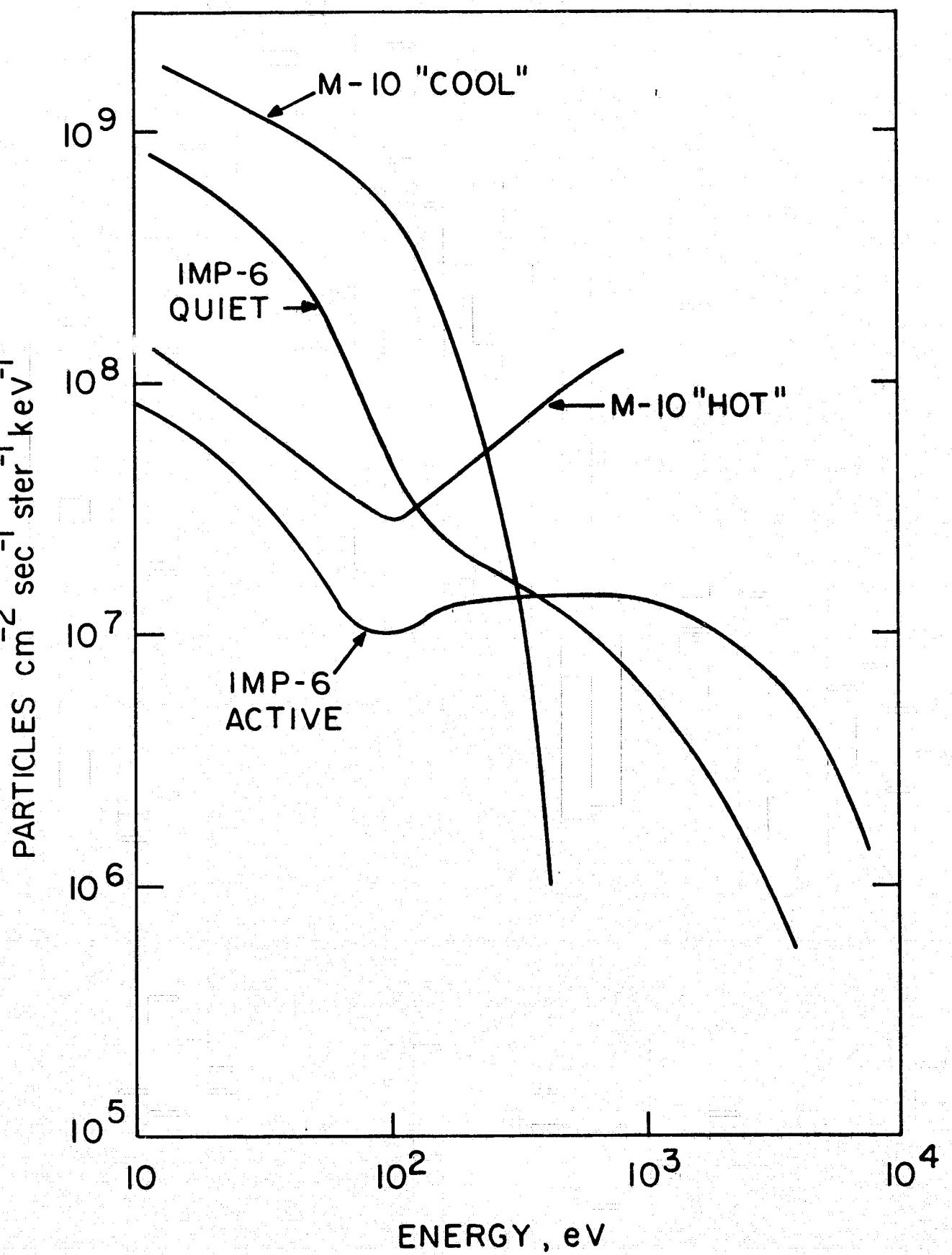
M-10 "COOL"
IMP-6
QUIET
M-10 "HOT"
IMP-6
ACTIVE
10^9
10^8
10^7
10^6
10^5
PARTICLES cm^{-2} sec^{-1} $ster^{-1}$ keV^{-1}
10
10^2
10^3
10^4
ENERGY, eV

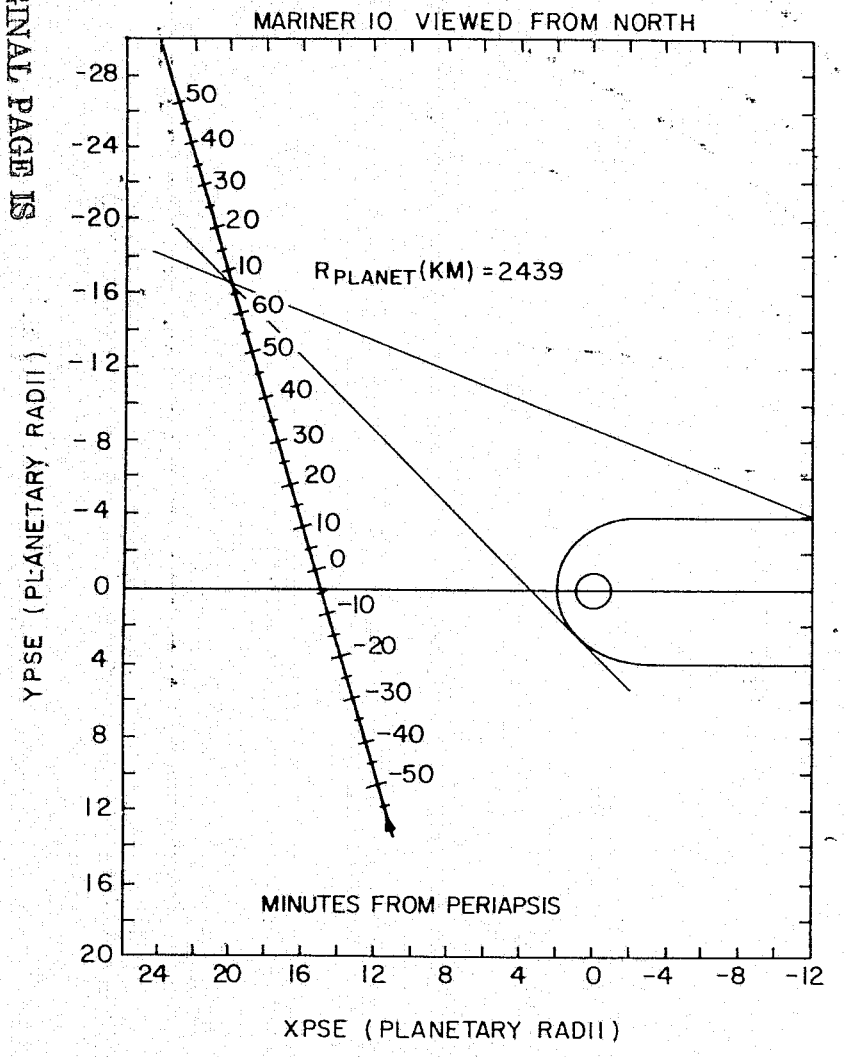

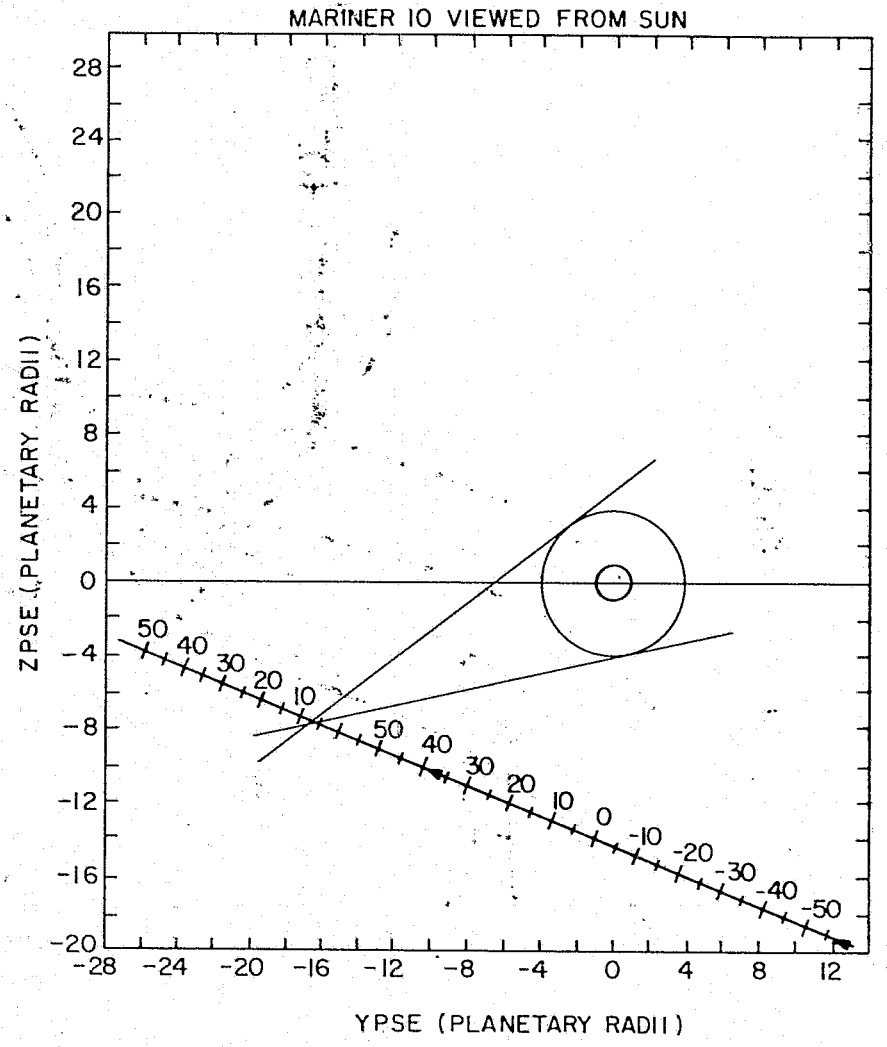

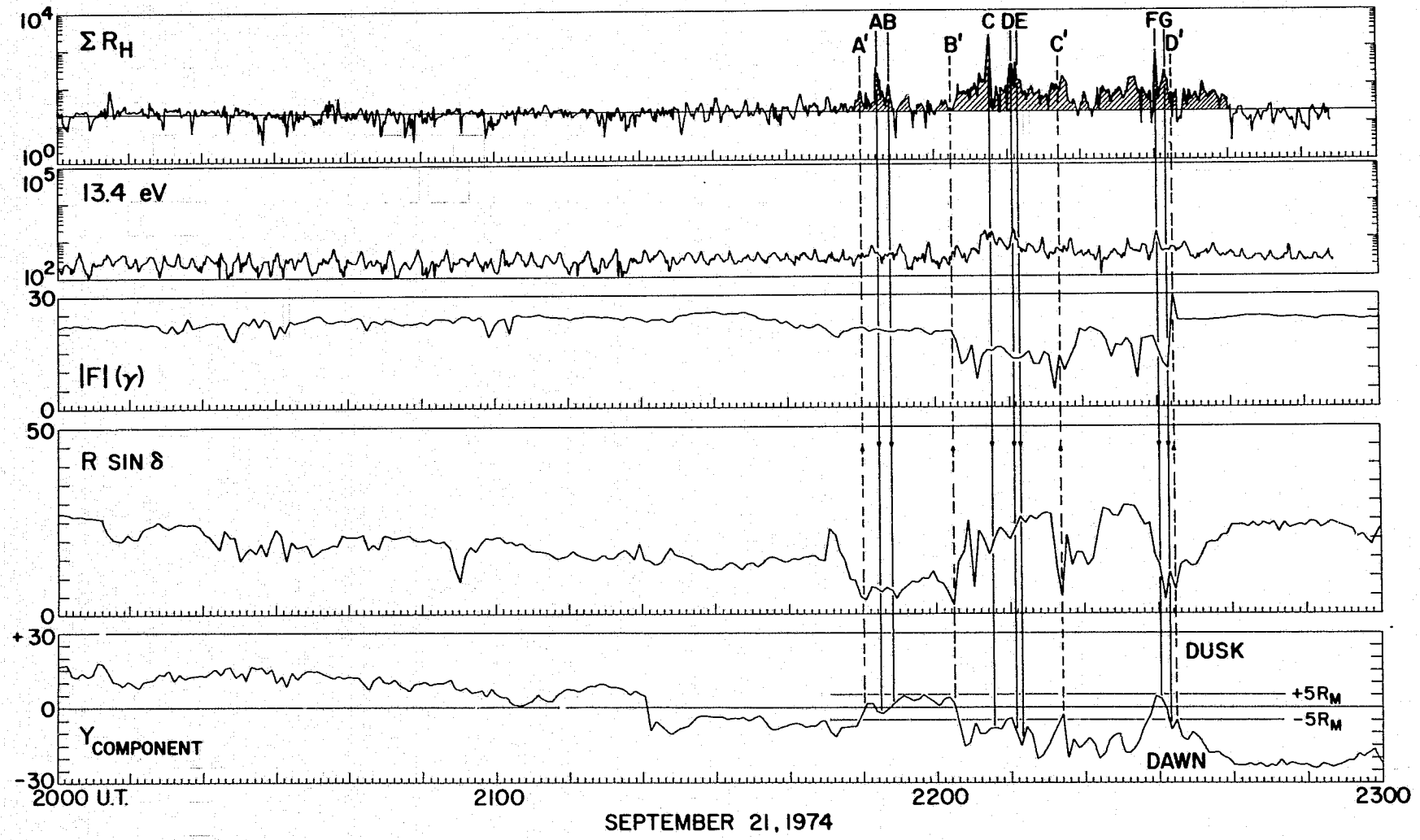
10^4
ΣR_H
A'
AB
B'
C
DE
C'
FG
D'
10^0
10^5
13.4 eV
10^2
30
|F| (γ)
0
50
R SIN δ
0
+30
DUSK
+5R_M
0
-5R_M
Y_COMPONENT
DAWN
-30
2000 U.T.
2100
2200
2300
SEPTEMBER 21, 1974

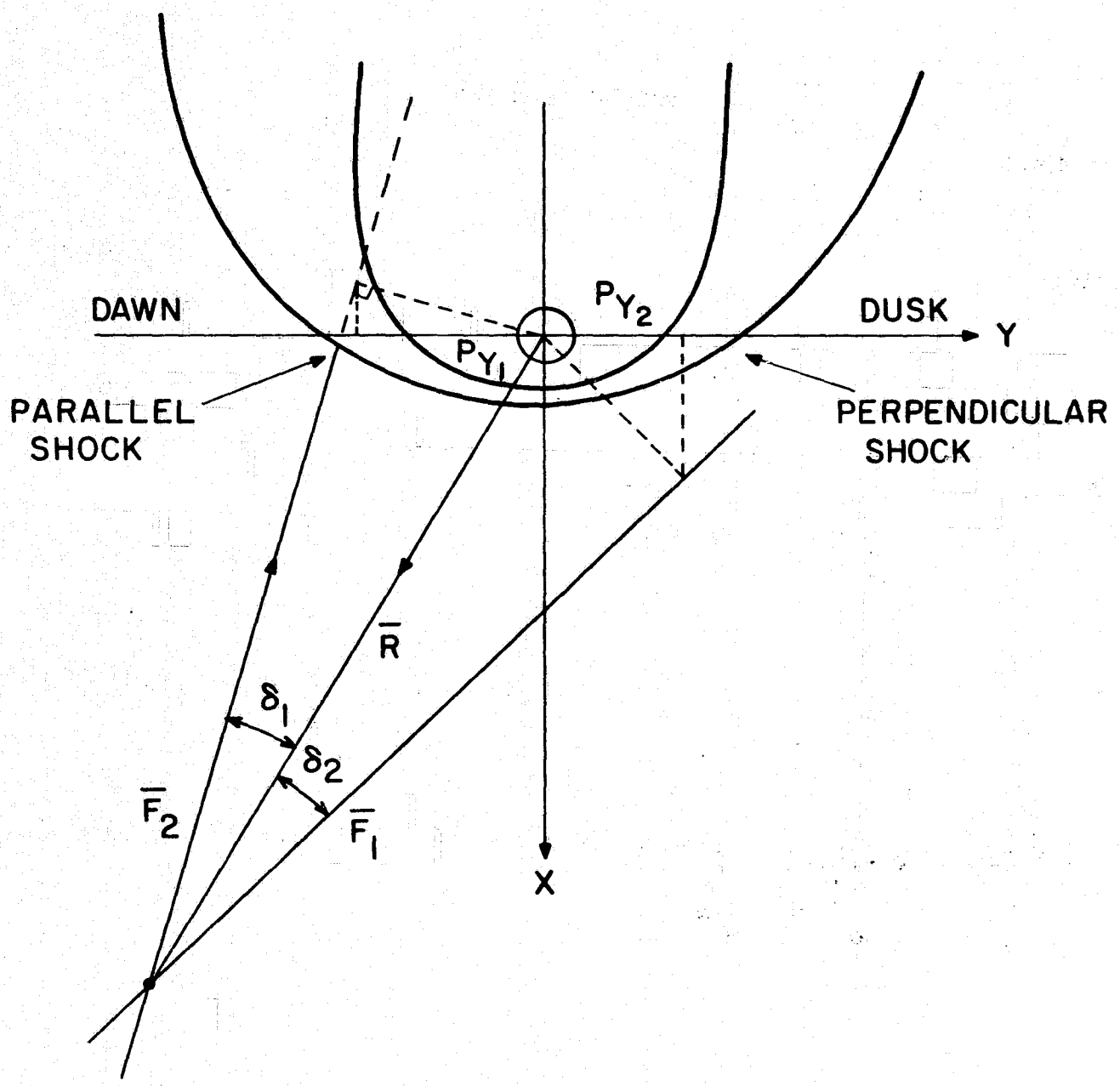
DAWN
DUSK
Y
P_{Y_2}
P_{Y_1}
PARALLEL SHOCK
PERPENDICULAR SHOCK
$\bar{R}$
δ_1
δ_2
$\bar{F}_2$
$\bar{F}_1$
X